GRB prompt emission modeling

Željka Bošnjak
University of Zagreb, Croatia

Sexten Center for astrophysics Riccardo Giacconi, June 30 - July 4, 2025

Outline

I - Leptonic and lepto-hadronic models for prompt GRB emission

II - GRB prompt emission from the synchrotron radiation of relativistic electrons and the low energy spectral slope

III - Distance measurements to dust clouds using GRB X-ray halos and the low energy spectrum reconstruction

IV - Off-axis MeV and very-high energy gamma-ray emissions from structured gamma-ray burst jets

Prompt emission models

What? What is the composition of a GRB jet? Is it predominantly composed of matter (baryons and leptons) or a Poynting flux?

Where? GRB emission should be internal, i.e. between the photosphere radius $R_{ph} \sim 10^{11} - 10^{12}$ cm and the deceleration radius, $R_{dec} \sim 10^{16} - 10^{17}$ cm

How? How is GRB emission produced? How the kinetic of Poynting flux energies get dissipated and converted to the internal energy, how the particles are accelerated, and how the photons are radiated?

TeV observations: decaying afterglows

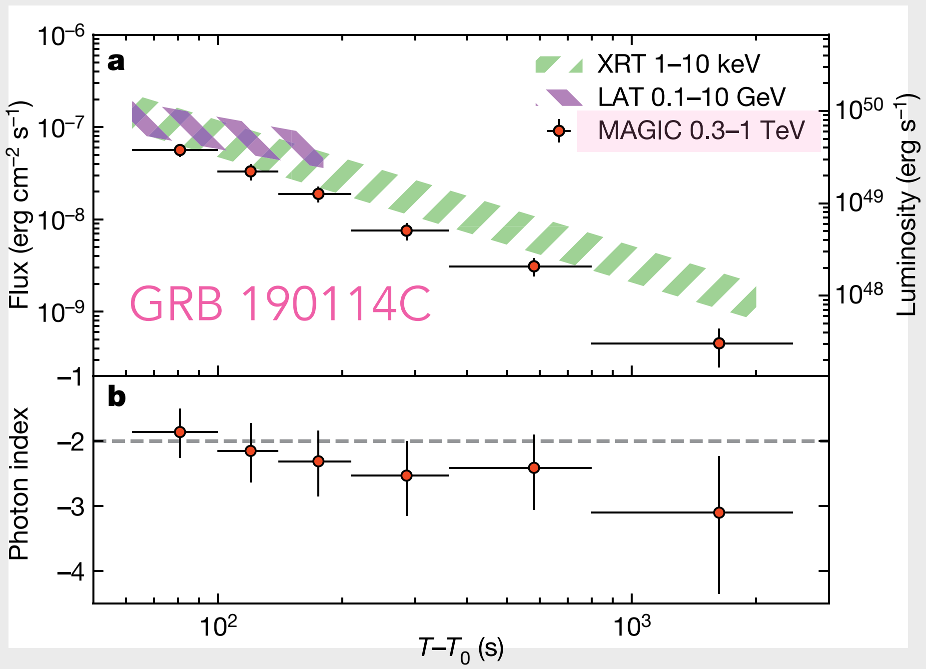

MAGIC collaboration 2019, Nature

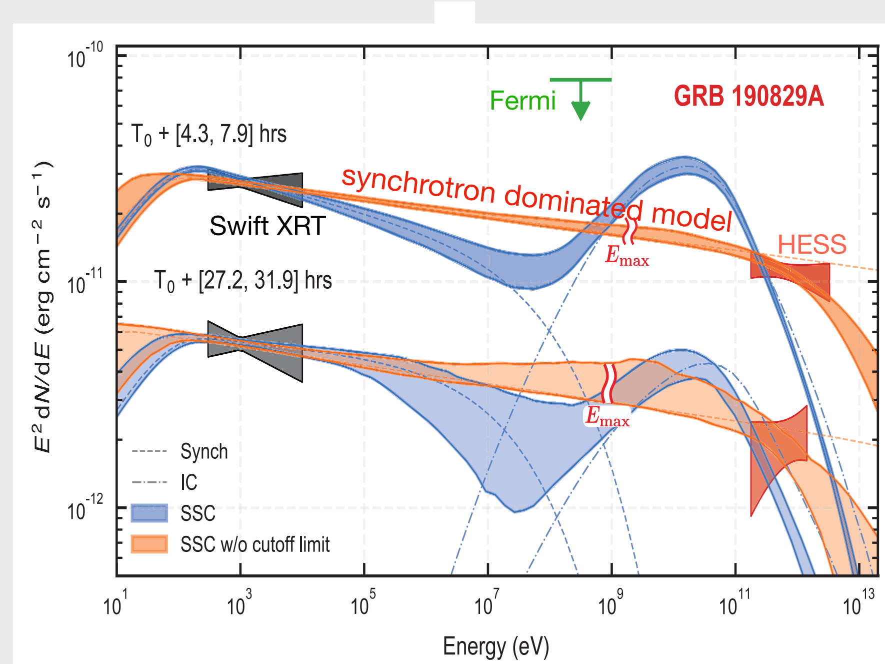

H.E.S.S. collaboration 2021, Science

GRB 160821B

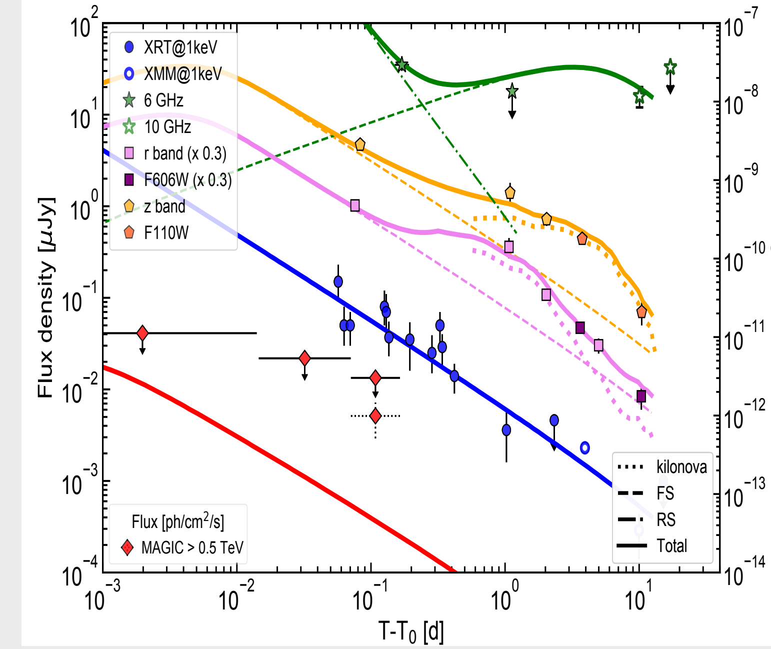

MAGIC collaboration, ApJ, 2021

MAGIC slew to the direction of GRB 190114C (z=0.42) about 50 s after the trigger and detected > 0.2 TeV photons

$E_{iso} \approx 3 \times 10^{53}$ erg

GRB 190829A: power law spectrum in the range (0.18-3.3) TeV $\gamma^{\rm int}_{\rm VHE}$=2.07

-low-luminosity GRB

-observed between 4 and 56 h after the trigger

z = 0.0785

$E_{iso} \approx 3 \times 10^{50}$ ergs

short GRB at z = 0.162

MAGIC observations started from 24 s after the trigger

Evidence of a gamma-ray signal above ~0.5 TeV until 4h after the burst

$E_{iso} \approx 1.2 \times 10^{49}$ erg

Talks by L. Nava, D. Miceli, A. Berti

TeV observations: GRB 221009A

First GRB seen by an extensive air shower detector

(LHAASO collaboration, Science 2023)

TeV light curve: a rise to peak after a quiescent phase, then a decay

$E_{iso} \sim 10^{55}$ erg   z = 0.151

First time detection of the afterglow onset?

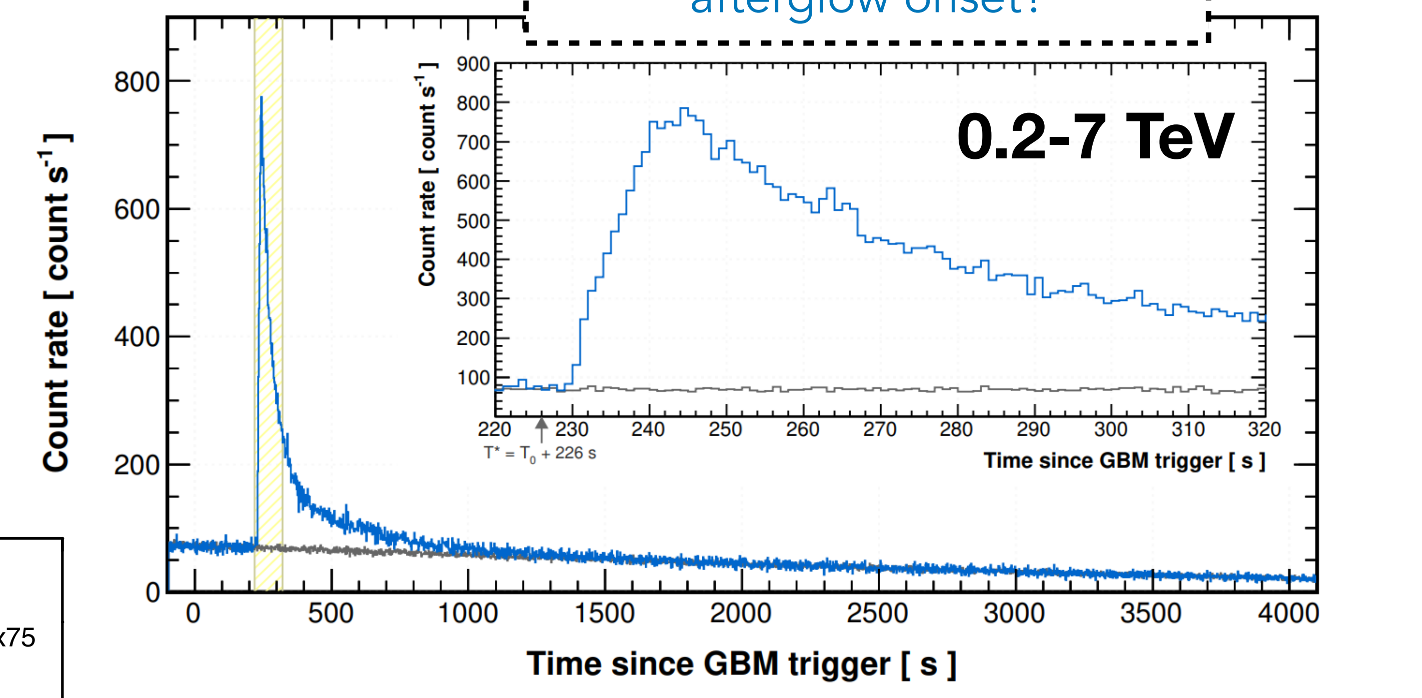

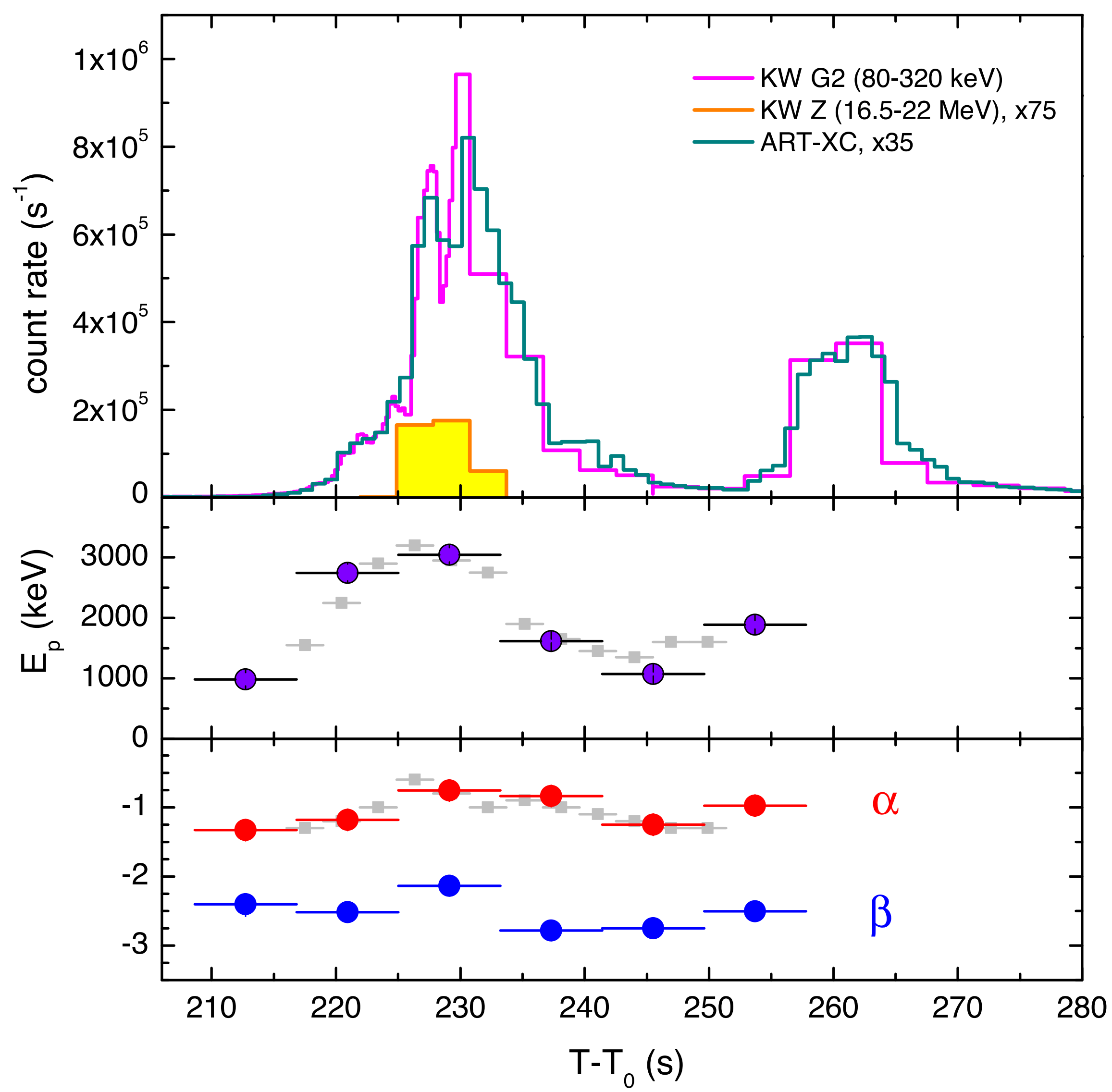

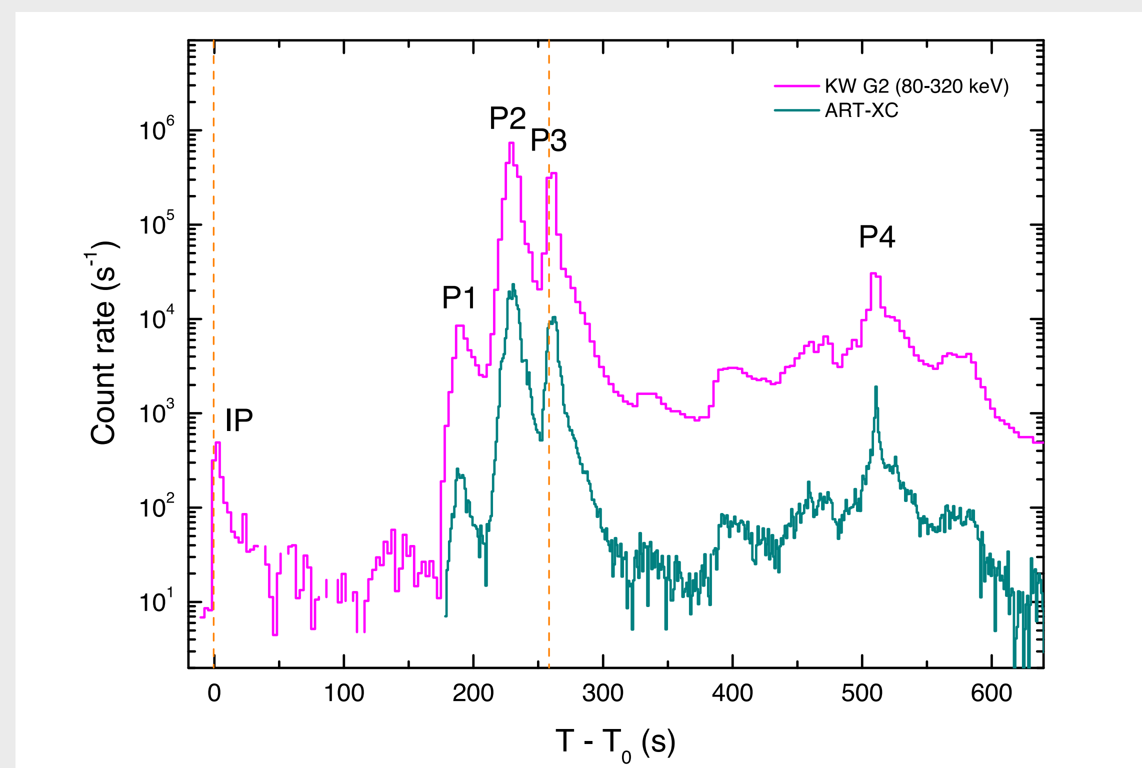

Frederiks et al. 2023: Konus-WIND and ART-XC (4- 30 keV) observations

SVOM and EP observational era

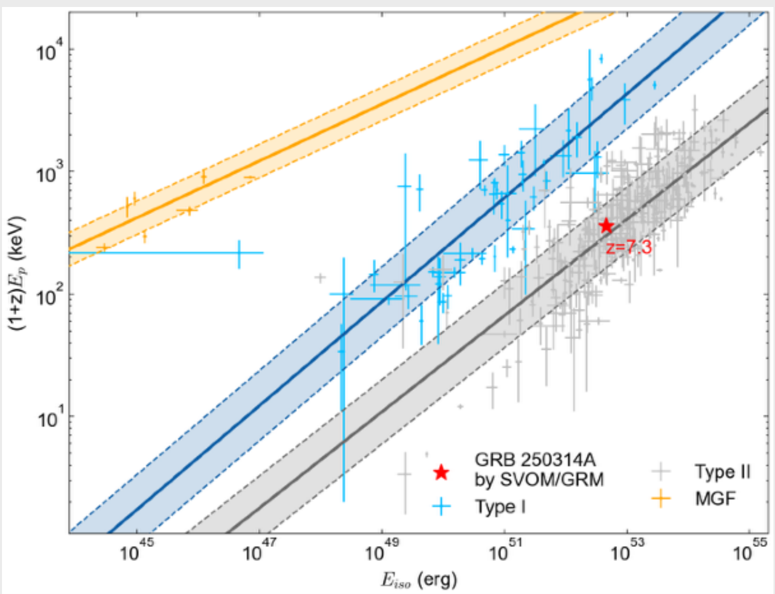

GCN Circular 39746

SVOM GRB 250314A: z ~ 7.3

(among the three most distant GRBs known)

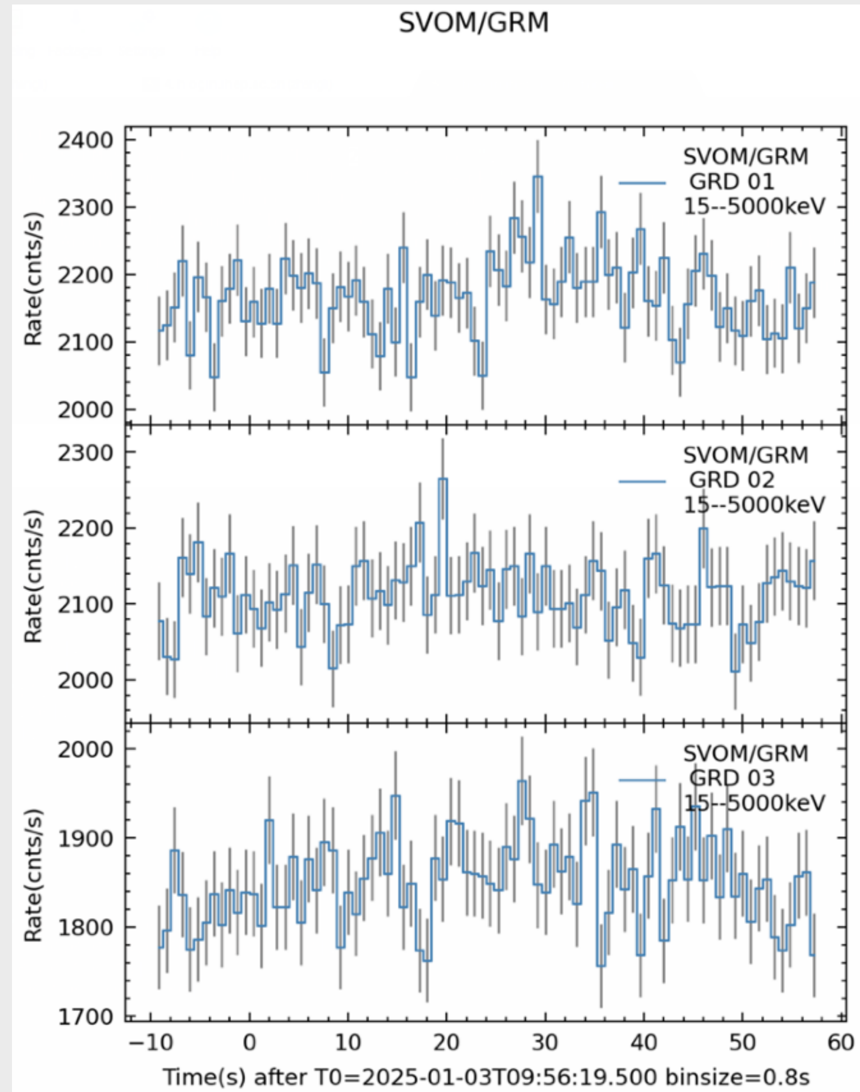

GCN Circular 38786

SVOM GRB 250103A: long duration GRB, $T_{90} > 250$ s (5-120 keV)

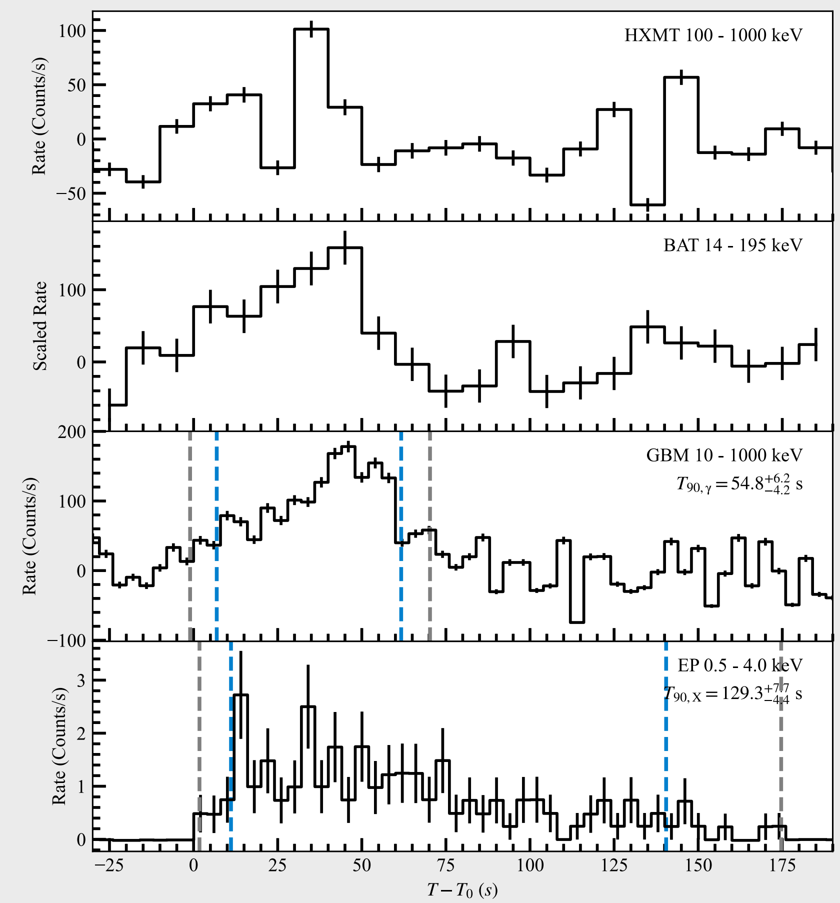

Yin et al. 2024

GRB 250103A: EP

$T_{90,\gamma}$ (10 - 1000 keV) ~ 55 s

$T_{90,X}$ (0.5 - 4 keV) ~ 129 s

Talk by F. Piron (SVOM)

Internal shock model: recent results

The jet is assumed to be weakly magnetized at large distance and the prompt emission is emitted above the photosphere by shock accelerated electrons.

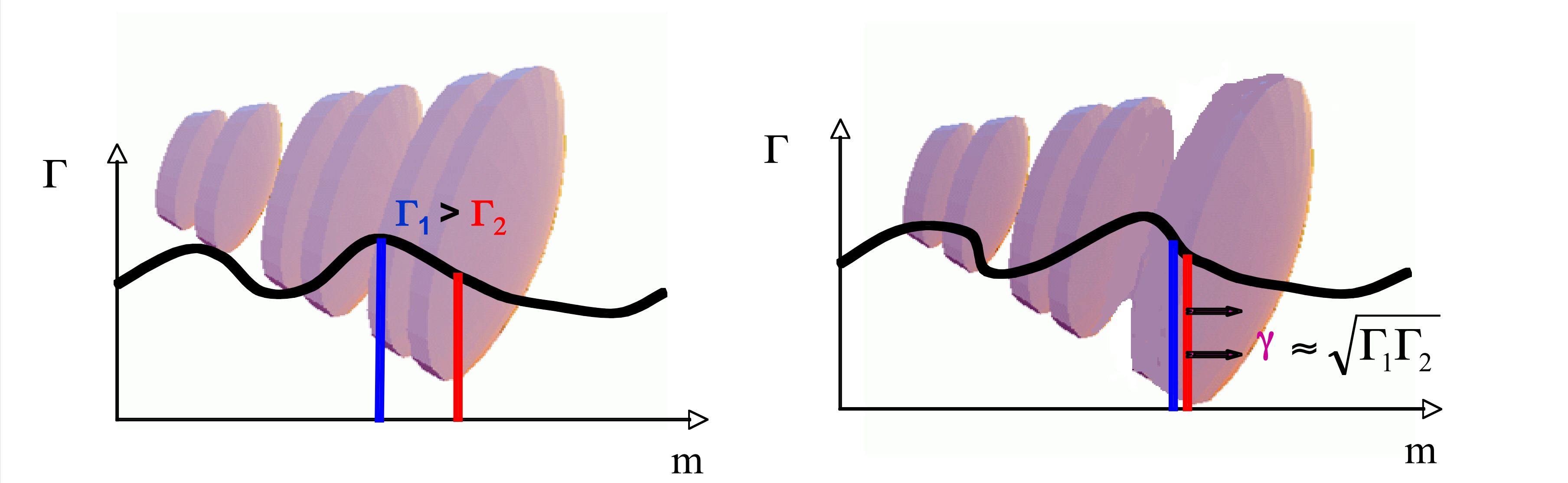

Piran 1999

Modeling:

1. dynamics of internal shocks

2. radiative processes in the shocked medium

3. observed spectra and time profiles

Bosnjak, Daigne & Dubus 2009
Daigne, Bosnjak & Dubus 2011
Bosnjak & Daigne 2014
Rudolph, Bosnjak, Palladino, Sadeh, Winter 2022
Rudolph, Petropoulou, Bosnjak, Winter 2023
Rudolph, Petropoulou, Winter, Bosnjak 2023
Daigne & Bosnjak 2025

Internal shock model

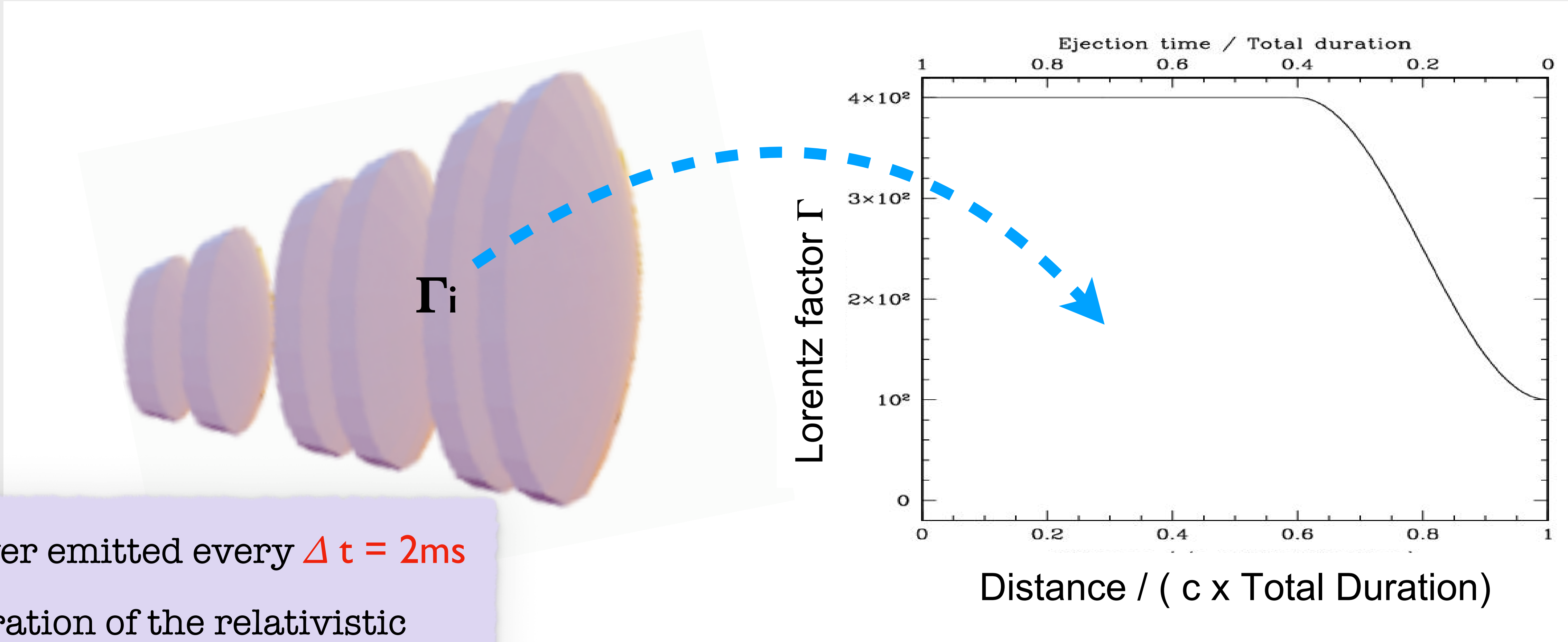

Layer emitted every Δt = 2ms

Duration of the relativistic ejection phase: $t_w \sim 2$ s

Number of shells: N = 1000

Layer mass: $M_i \sim 1 / \Gamma_i$

Shortest timescale of variability: t_{var}

$R_{IS,\,start} \sim \Gamma\ c t_{var} \sim 3 \times 10^{11}$ cm $(\Gamma/100)$ $(t_{var}/1\ \mathrm{ms})$

$R_{IS,\,end} \sim \Gamma\ c t_w \sim 3 \times 10^{15}$ cm $(\Gamma/100)$ $(t_w/10\ \mathrm{s})$

Dissipated energy: from 6% $(\Gamma_2 / \Gamma_1 = 2)$ to 43 % $(\Gamma_2 / \Gamma_1 = 10)$

Daigne & Mochkovitch 2000: the simplified approach for dynamics has been confirmed by comparison with a full hydrodynamical calculation

Internal shock model

Physical conditions in the shocked medium: Lorentz factor $\boldsymbol{\Gamma^*}$, comoving density ρ^*, comoving specific energy density ε^*

$$R_{\rm is} \simeq \frac{8\kappa^2}{(\kappa-1)(\kappa+1)^3}\bar{\Gamma}^2 c\tau$$

$$\Gamma_* \simeq \frac{2\sqrt{\kappa}}{1+\kappa}\bar{\Gamma},$$

$$\rho_* \simeq \frac{\dot{E}}{4\pi R_{\rm is}^2\Gamma_*^2 c^3},$$

$$\epsilon_* \simeq \frac{\left(\sqrt{\kappa}-1\right)^2}{2\sqrt{\kappa}}c^2.$$

$$n_{\rm e}^{\rm acc} \simeq \zeta\frac{\rho_*}{m_{\rm p}}$$

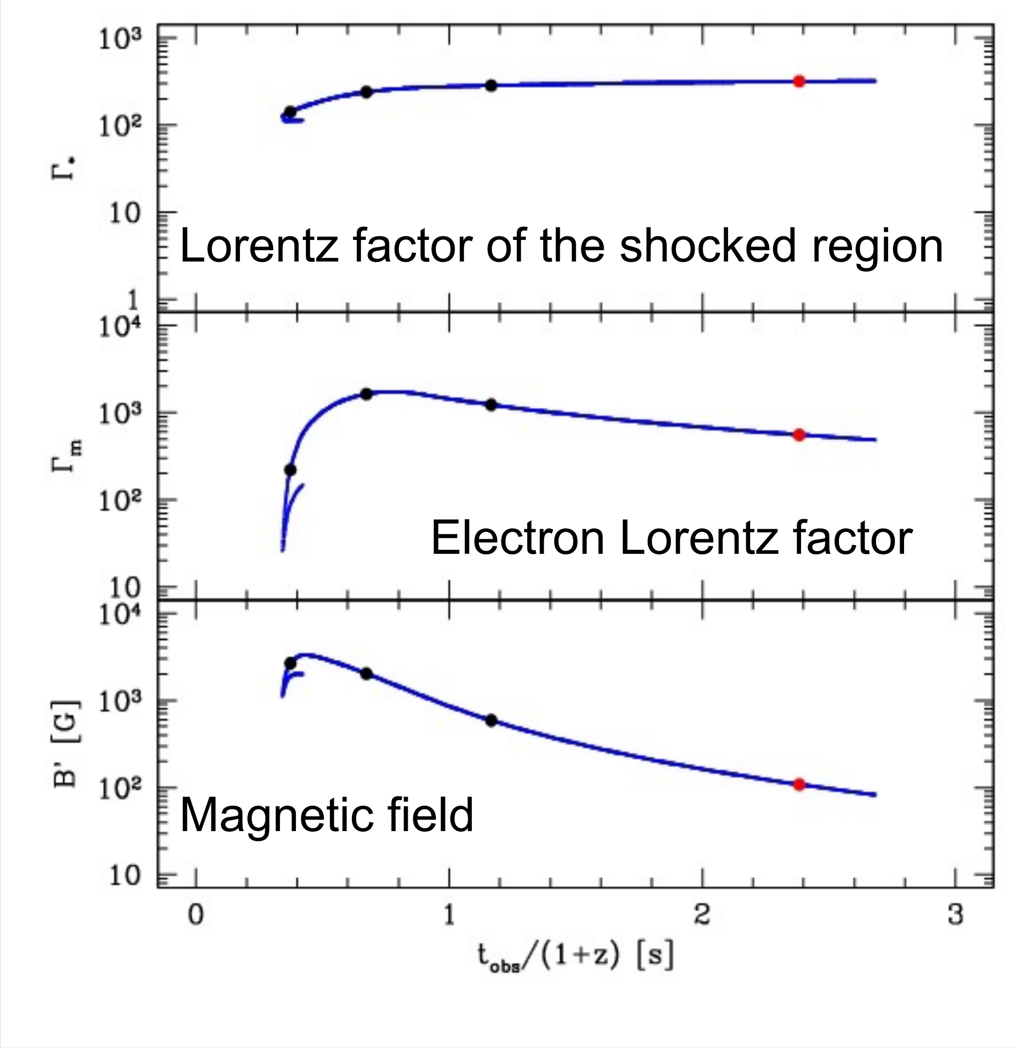

Internal shock model

Physical conditions in the shocked medium: Lorentz factor $\mathbf{\Gamma^*}$,

comoving density ρ^*, comoving specific energy density ε^*

Relativistic electron density:

$$n(\gamma) \simeq (p-1)\frac{n_e^{acc}}{\Gamma_m}\left(\frac{\gamma}{\Gamma_m}\right)^{-p} \quad \text{for } \gamma \geq \Gamma_m$$

$\zeta < 1$ of all electrons is accelerated

$$\Gamma_m \simeq \frac{p-2}{p-1}\frac{\epsilon_e\,\rho_*\epsilon_*}{n_e^{acc} m_e c^2} \simeq \frac{p-2}{p-1}\frac{\epsilon_e}{\zeta}\frac{m_p}{m_e}\frac{\epsilon_*}{c^2}\,.$$

$$B' \simeq \sqrt{8\pi\epsilon_B\,\rho_*\epsilon_*}\,.$$

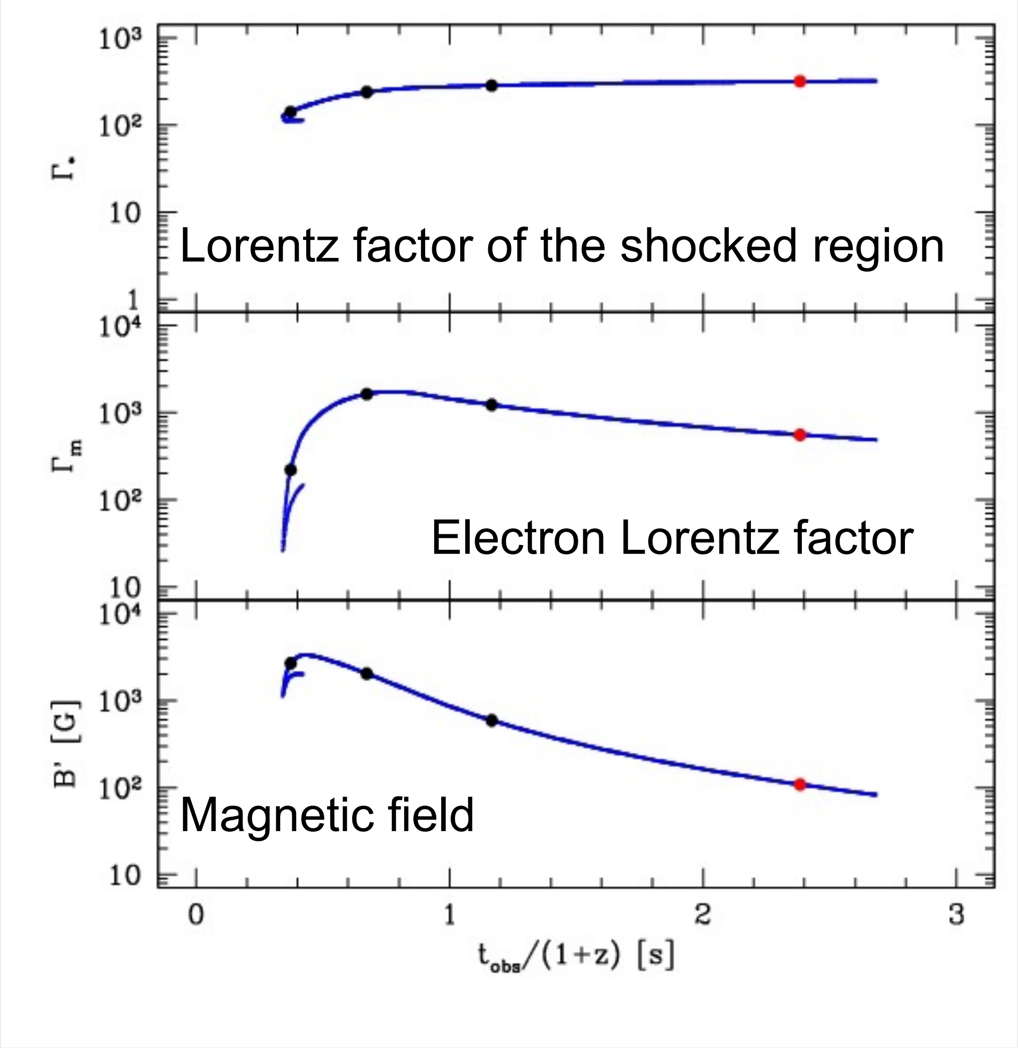

Dissipated energy is distributed between protons, electrons (fraction ε_e) and magnetic field (fraction ε_B)

Internal shock model

Radiation: the time evolution of electrons and photons in the comoving frame is solved (time-dependent radiative code)

Comptonization parameter
$Y = L_{ic} / L_{syn}$

IC dominant:
low frequency synchrotron peak
Thomson regime

Synchrotron dominant:
high frequency synchrotron peak
Klein-Nishina regime

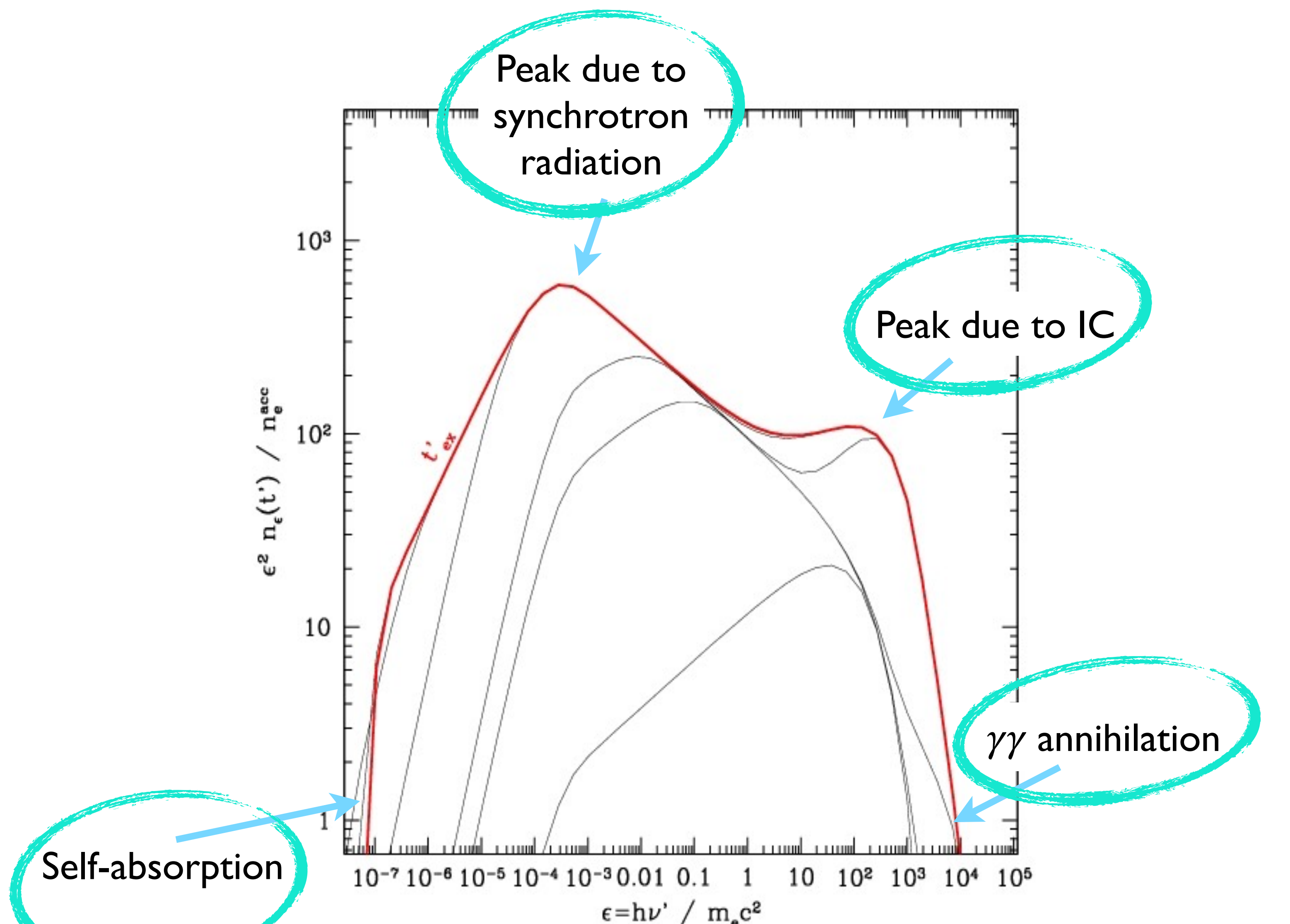

Emitted photon spectrum

This calculation is done at all times along the propagation of each shock wave

All the contributions are added together to produce a synthetic gamma-ray burst (spectrum+lightcurve)

Synchrotron spectrum

Briggs et al. 1999

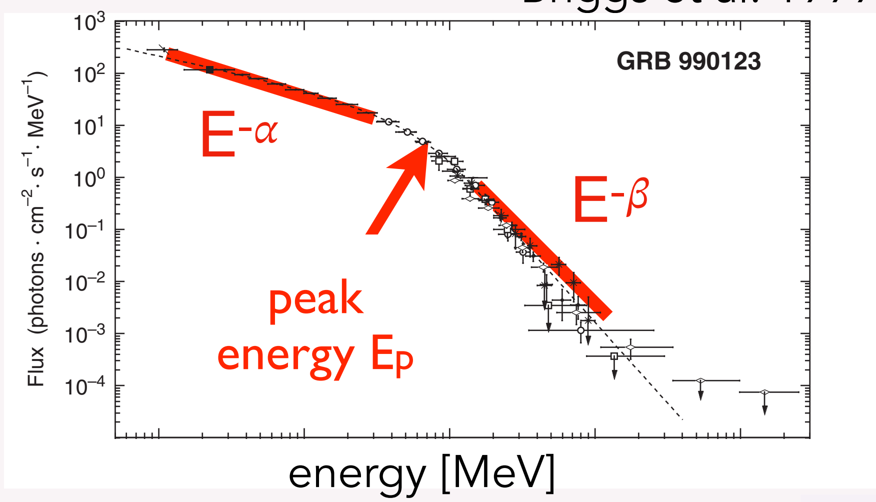

Relativistic electrons:

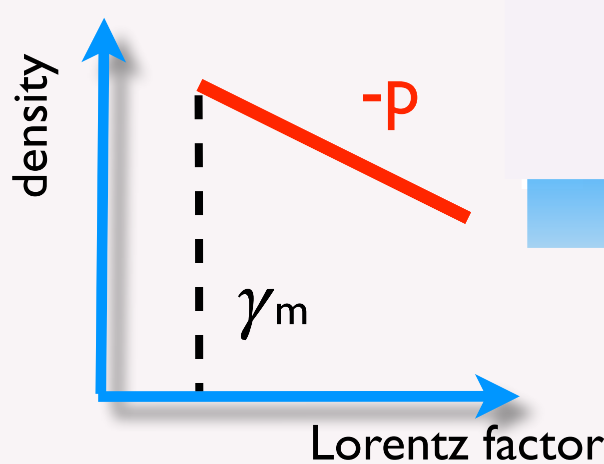

Sari, Piran & Narayan 1998

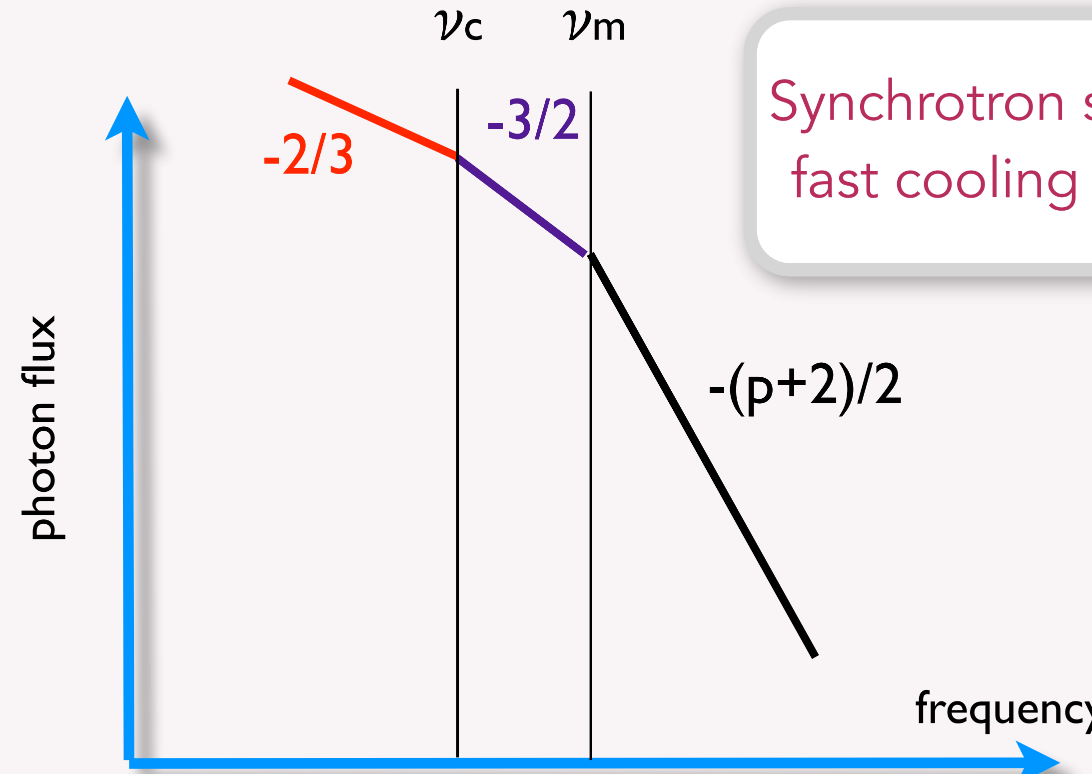

Synchrotron spectrum: fast cooling ($\gamma_c < \gamma_m$)

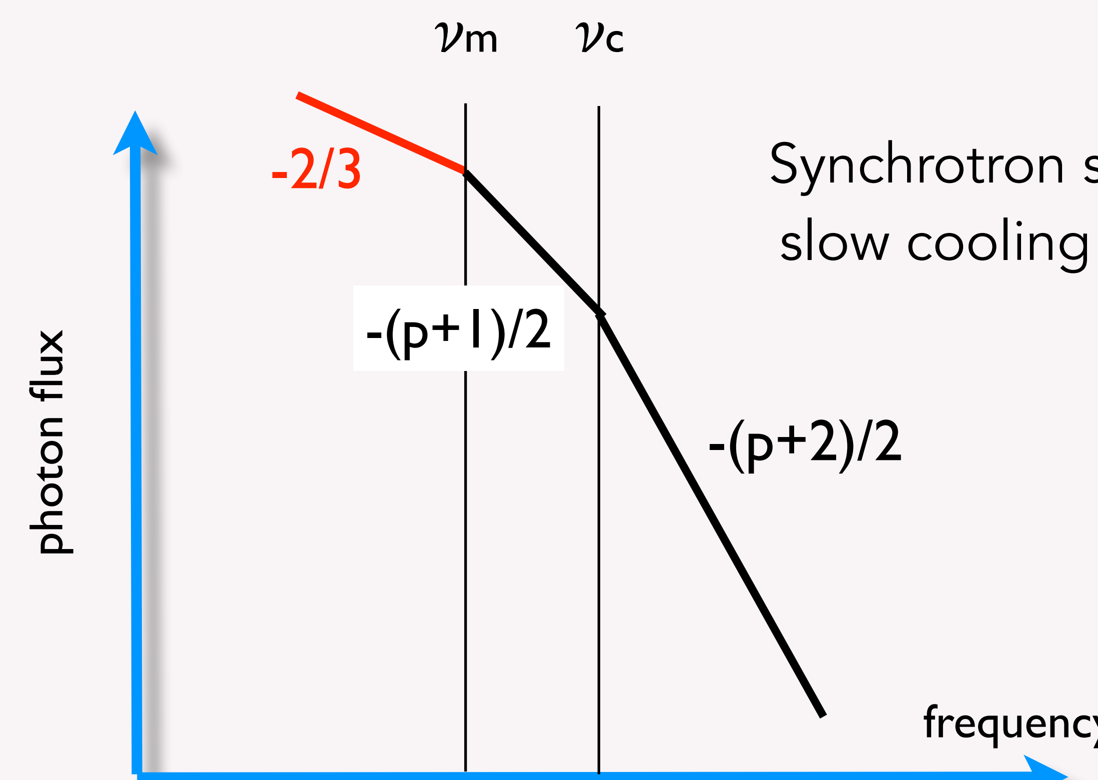

Synchrotron spectrum: slow cooling ($\gamma_c > \gamma_m$)

γ_m: minimum Lorentz factor at injection

γ_c: radiative timescale = dynamical timescale

Synchrotron spectrum

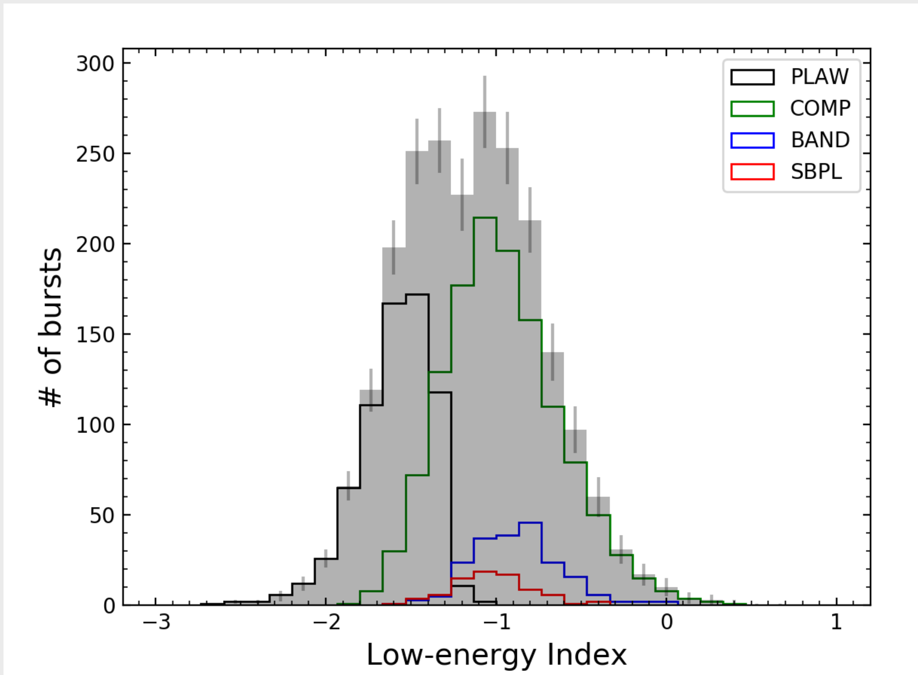

Time-integrated spectral fits: $\alpha = -1.08^{+0.45}_{-0.44}$

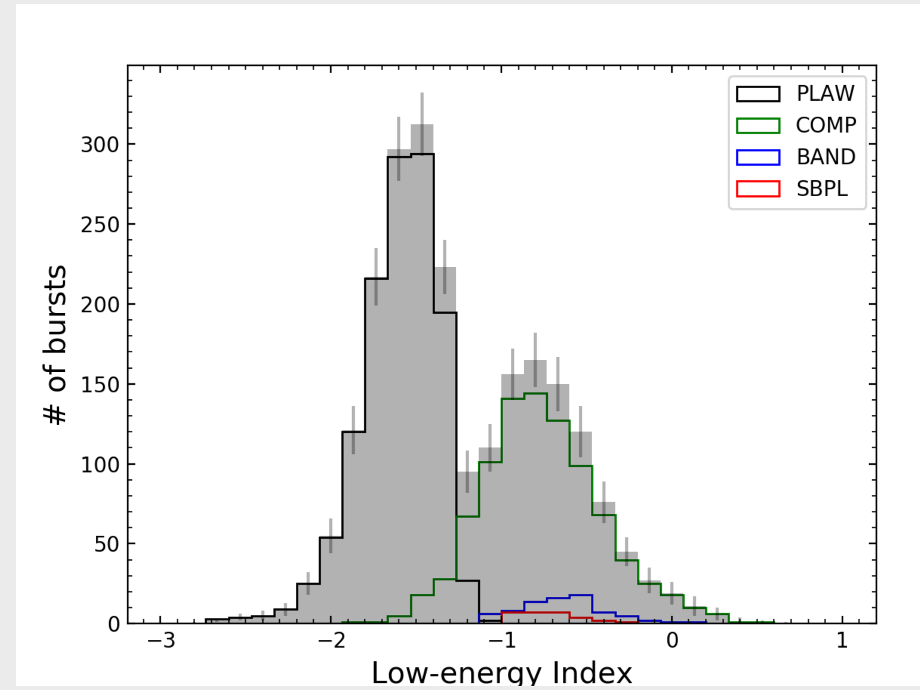

Peak-flux spectral fits: $\alpha = -1.30^{+0.77}_{-0.33}$

Poolakkil et al. 2021

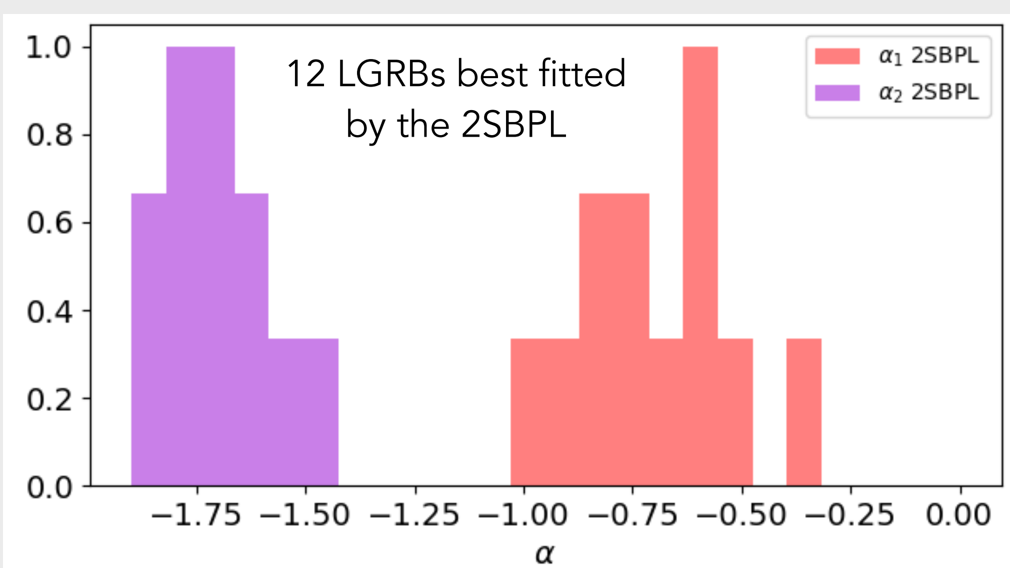

Toffano et al. 2021: 12 LGRBs observed by Fermi GBM, having large fluences and large E_{peak} values

→ the distributions of spectral slopes peak at -0.71 and -1.71, not far from the typical values -2/3 and -3/2 expected for synchrotron spectrum from marginally fast cooling electrons

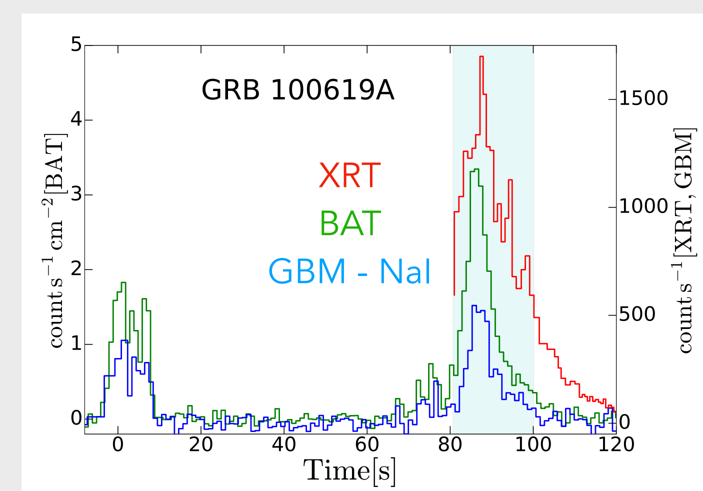

Oganesyan et al. 2018; 2017
joint XRT+BAT spectral analysis for 34 GRBs

Steep low-energy slopes

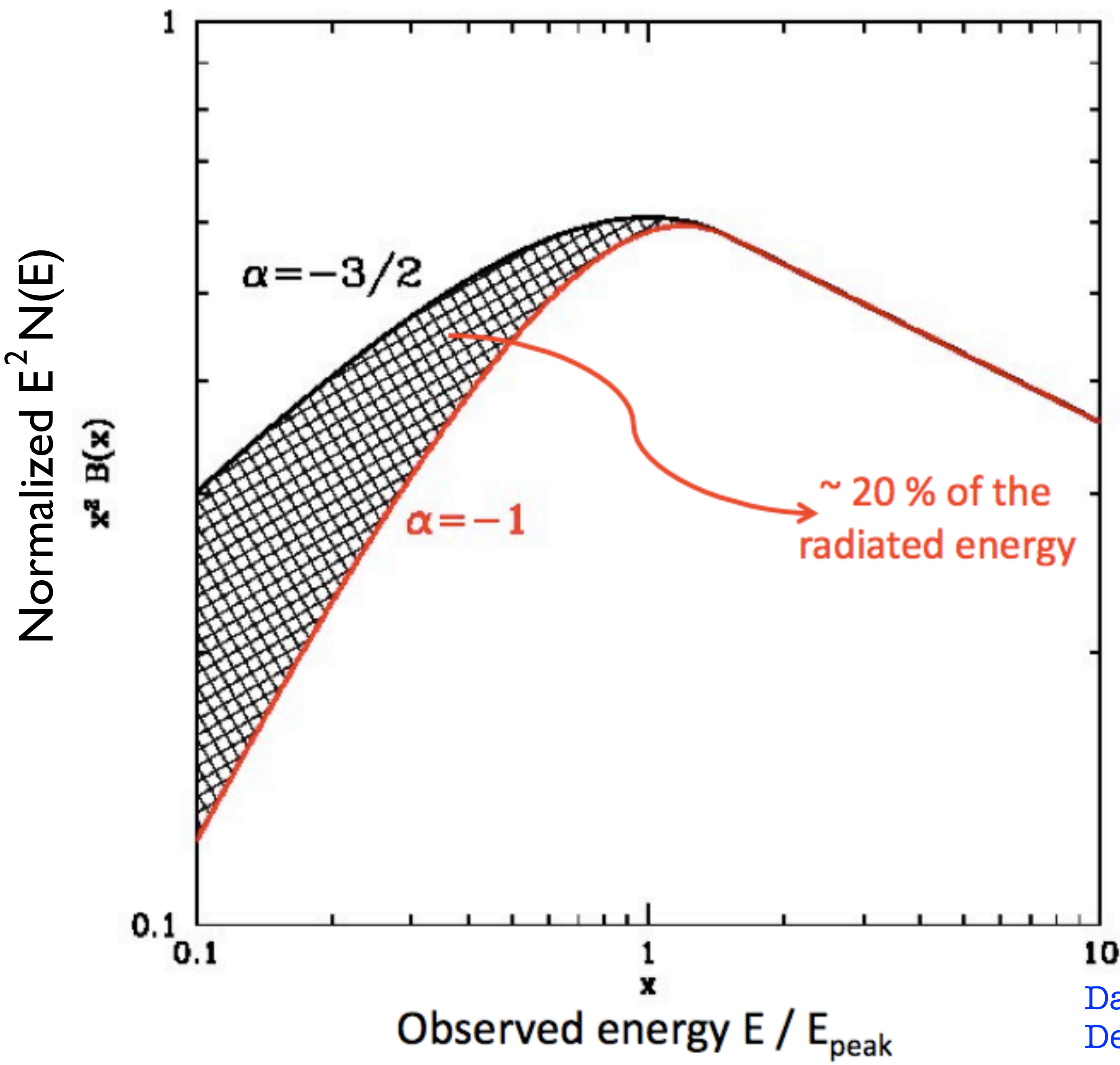

Band function

α = - 1.5 $\longrightarrow$ -1

β = - 2.25

Inverse Compton scatterings in Klein-Nishina regime have an impact on the synchrotron slope

Daigne, Bosnjak & Dubus 2011
Derishev 2001

Steep low-energy slopes

- synchrotron emission + IC scatterings in the Klein-Nishina regime: $\alpha \rightarrow -1$ but not much steeper

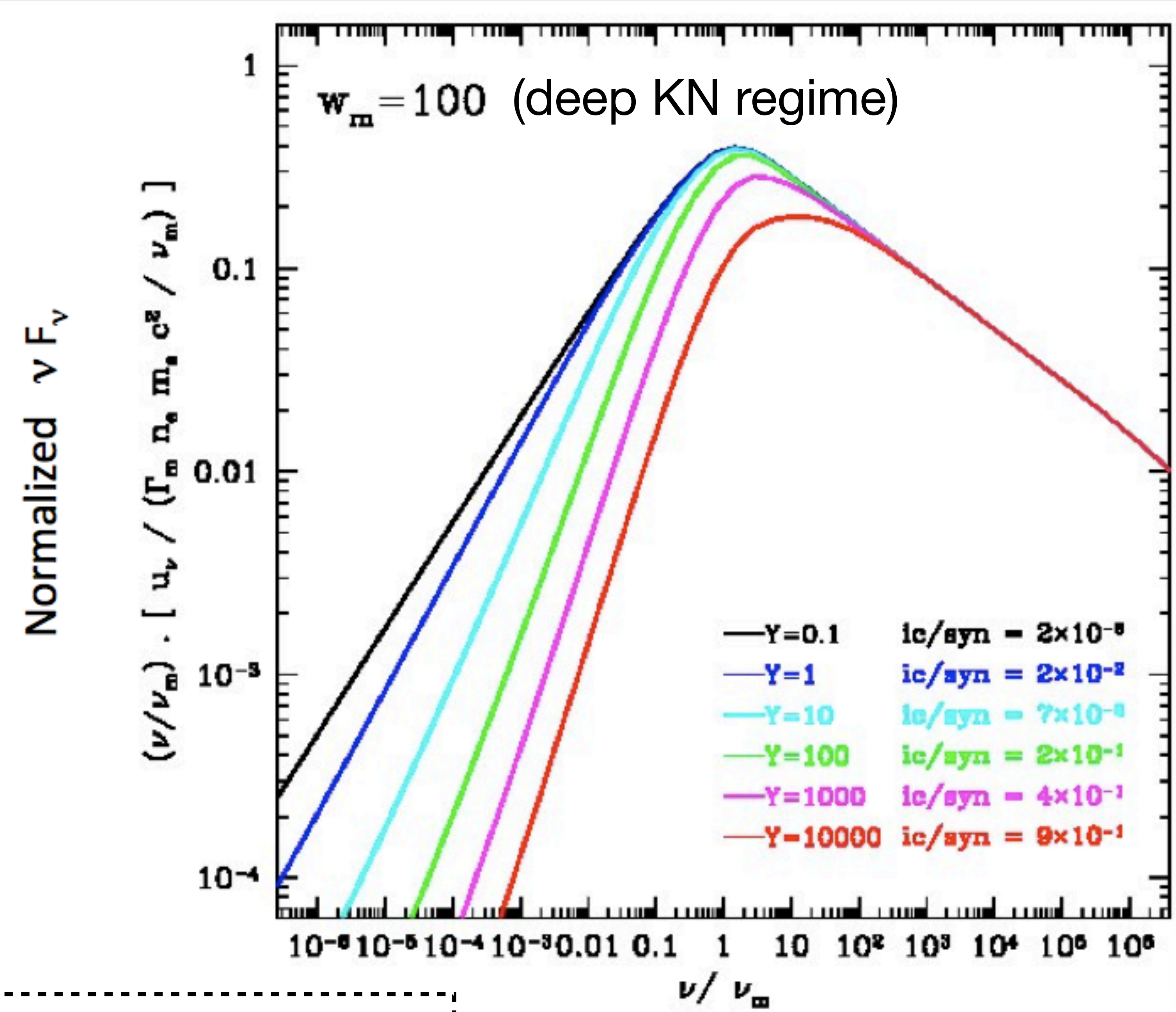

w_m : importance of KN

$$w_{\rm m} = \Gamma_{\rm m} \frac{h\nu'_{\rm m}}{m_{\rm e}c^2}$$

Y : importance of IC vs syn

$$Y = \frac{4}{3}\tau_{\rm T}\Gamma_{\rm m}\Gamma_{\rm c} \simeq \frac{\epsilon_{\rm e}}{\epsilon_{\rm B}}$$

Thomson regime: the electron cooling rate due to IC scatterings remains proportional to γ^2 as for the synchrotron power

KN regime: the electron cooling rate due to IC depends on γ

Daigne, Bosnjak, Dubus 2011
Derishev 2001
Nakar et al. 2009

Exact calculation with synchrotron + IC only
(no adiabatic cooling, synchrotron self-absorption, γγ annihilation)

Multi-wavelength radiation model for low-luminosity GRBs, and the implications for UHECRs

Rudolph, ŽB, Palladino, Sadeh, Winter 2022

▸ Motivation

LL GRBs are fainter about four orders of magnitude ($L \lesssim 10^{49}$ erg/s) from the commonly observed long GRBs

relatively soft ($E_p \lesssim 100$ keV)

not highly beamed (e.g. Soderberg 2006)

low Lorentz factors ($\Gamma \lesssim 50$) (e.g. Cano et al. 2017)

in some cases exhibit substantially longer durations (up to several 10^3 s)

Their low luminosity limits the detection to a distance of ~ 100 Mpc, but LL GRBs are much more common than long GRBs (Liang et al. 2007)

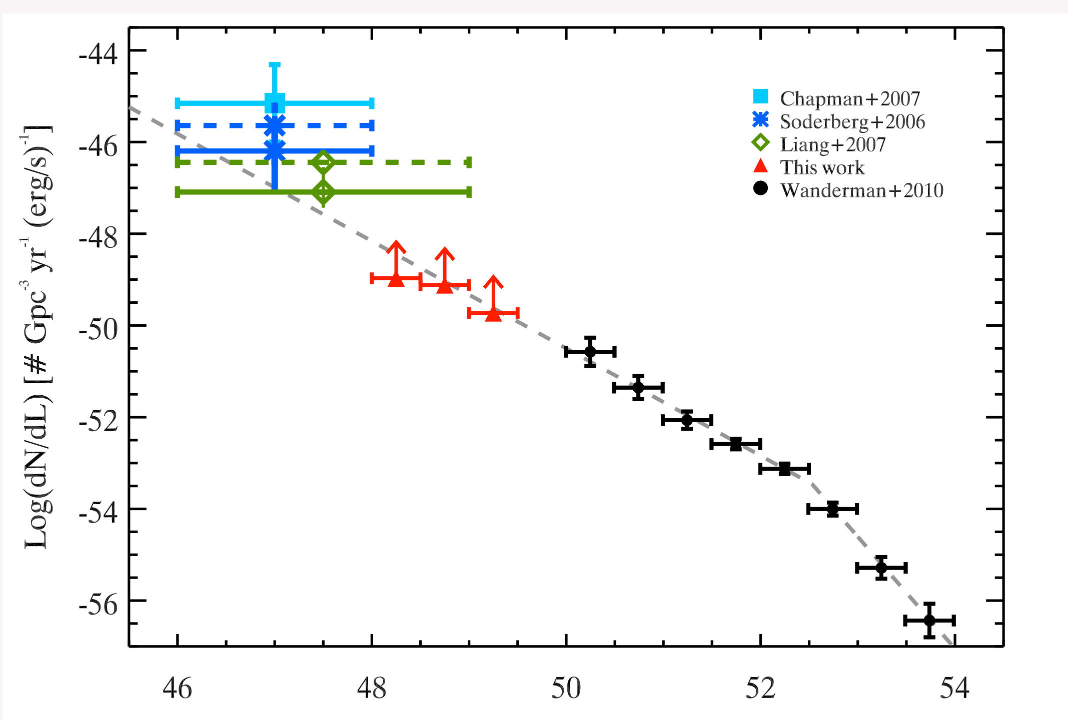

Pescalli et al. 2015

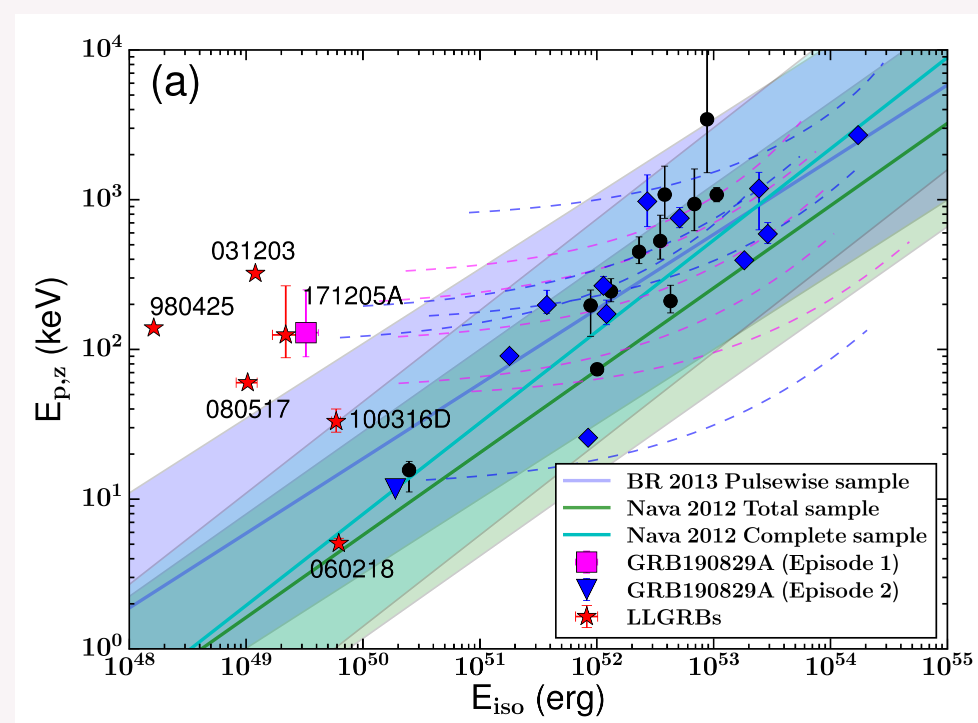

Chand et al. 2020

Ghisellini, Ghirlanda, Mereghetti, ŽB et al. 2006

Multi-wavelength radiation model for low-luminosity GRBs, and the implications for UHECRs

- **Motivation**

LL GRBs have been proposed as sources of cosmic rays and neutrinos

(Murase et al. 2006; 2008, Zhang et al. 2018; Boncioli et al. 2019; Samuelsson et al. 2020):

they are likely to have a much higher event rate in the local universe + heavy nuclei much easily survive inside the sources due to their lower radiation luminosity

→ LL GRBs are of special interest, both for the understanding of GRBs and their connection to SNe, and as sources of HE non-electromagnetic signals such as GWs

Multi-wavelength radiation model for low-luminosity GRBs, and the implications for UHECRs

- **Models**

Long GRBs seen off-axis: Pescalli et al. 2015; Aloy et al. 2018

Relativistic shock breakouts: Bromberg et al. 2011; Nakar & Sari 2012; Nakar 2015

Mildly relativistic jets seen on-axis: Daigne & Mochkovitch 2007; Zhang et al. 2012; Irvin & Chevalier 2016

Constraints:

→ relativistic breakouts may take place in choked GRBs, where the relativistic jets fail to penetrate through the stellar envelope, and no regular long GRB is produced (Nakar & Sari 2012).

The relativistic shock-breakout model predicts a 'fundamental plane' correlation

$$T_{90} \sim 20\ \mathrm{s}\,(1+z)^{-1.68}(E_{\gamma,\mathrm{iso}}/10^{46}\ \mathrm{erg})^{1/2}(E_{\mathrm{p}}/50\,\mathrm{keV})^{-2.68}$$

Nakar & Sari 2012

For GRB 120422A:

the predicted shock-breakout duration ~1100s

T_{90} ~ 5 s

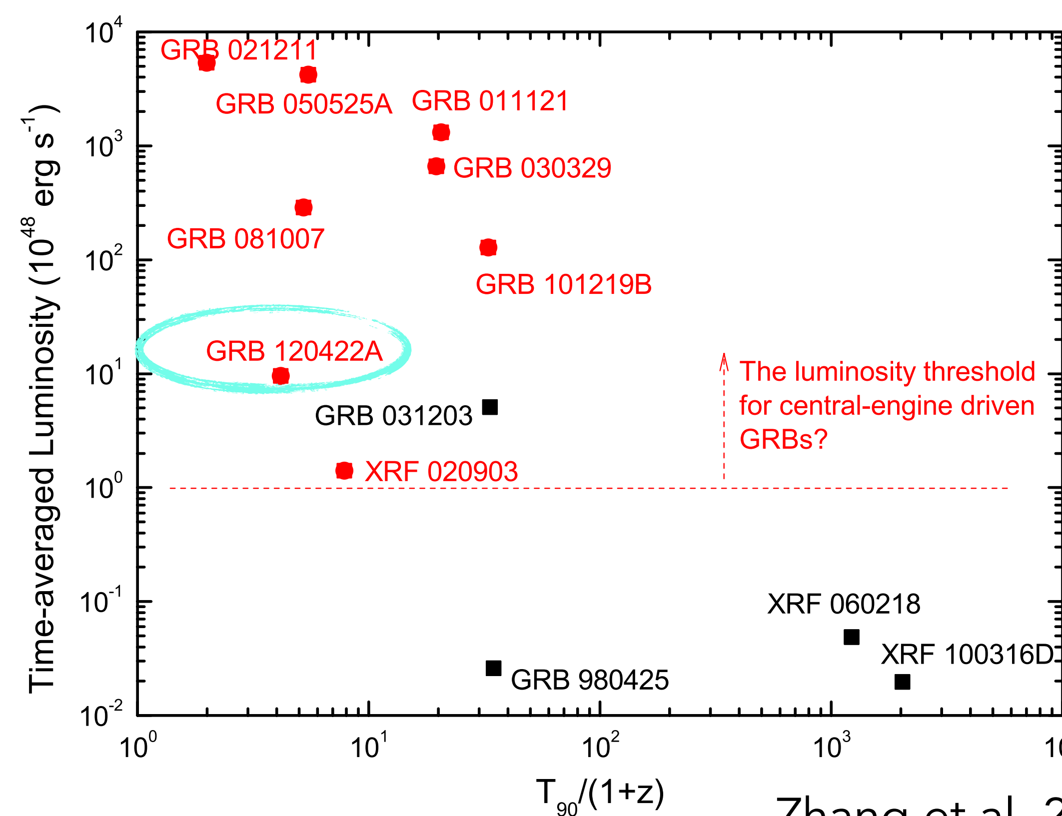

Zhang et al. 2012

Reference GRBs

GRB 980425

GRB100316D

GRB120714B

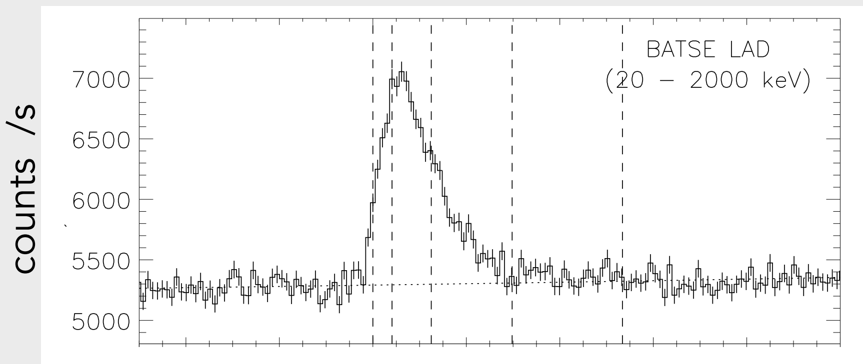

Kaneko et al. 2006

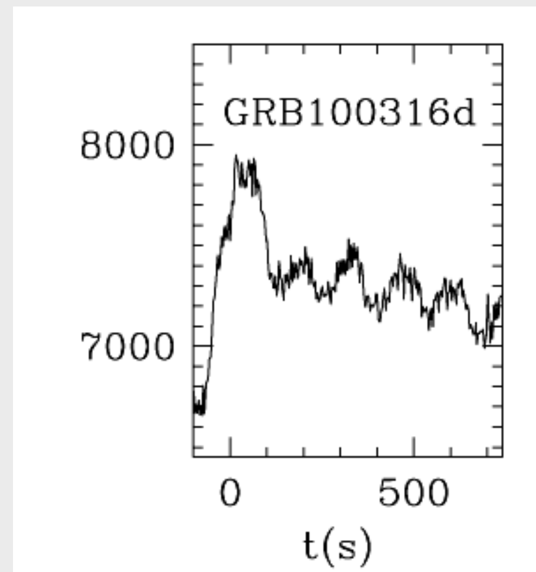

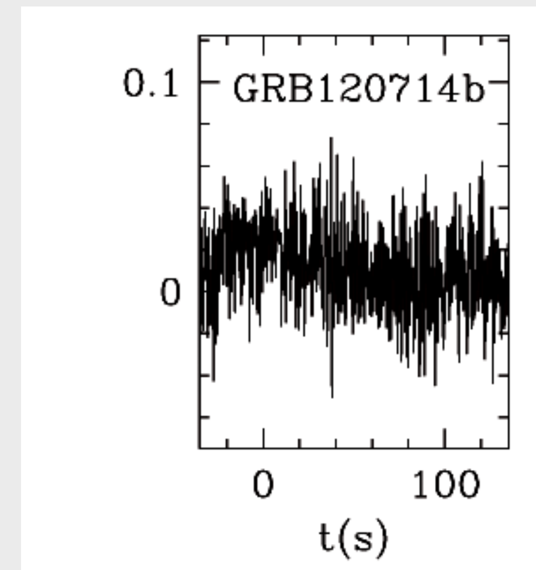

Swift BAT archive; swift.gsfc.nasa.gov

Model inputs:

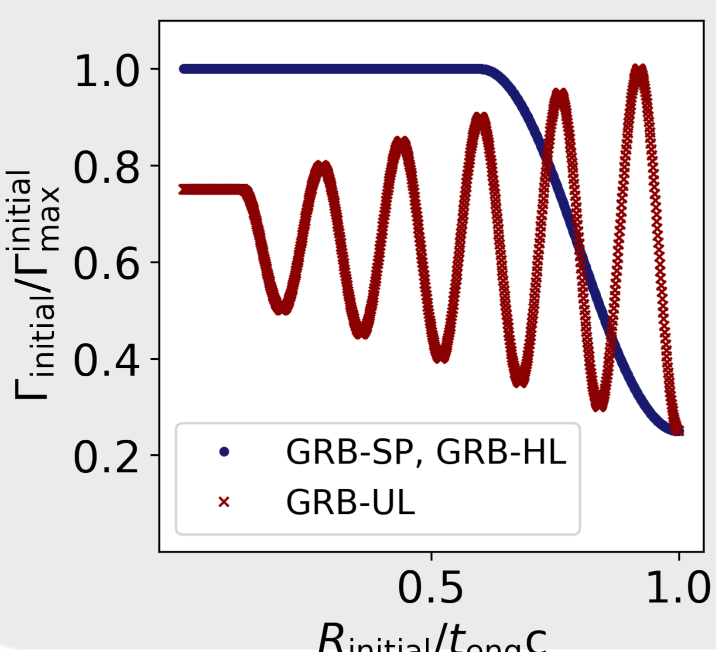

		GRB 980425	GRB 100316D	GRB 120714B
Observed	$E_{\gamma,\,\mathrm{iso}}$ (erg)	$1.6 \cdot 10^{48}$	$3.9 \cdot 10^{49}$	$5.9 \cdot 10^{50}$
	T_{90} (s)	35	1300	159
	E_{peak} (keV)	122	30	101
	z	0.0085	0.059	0.3984
		sp-GRB	ul-GRB	hl-GRB
Input	$\Gamma_{\mathrm{initial,\,max}}$, $\Gamma_{\mathrm{initial,\,min}}$	40, 10	40, 10	80, 20
	L_{wind} (erg s^{-1})	$2.5 \cdot 10^{48}$	$5.8 \cdot 10^{48}$	$3 \cdot 10^{50}$
	N_{shells}	1000	1000	1000
	t_{eng} (s)	40	1000	130

Rudolph, ŽB, Palladino, Sadeh, Winter 2022

Reference GRBs

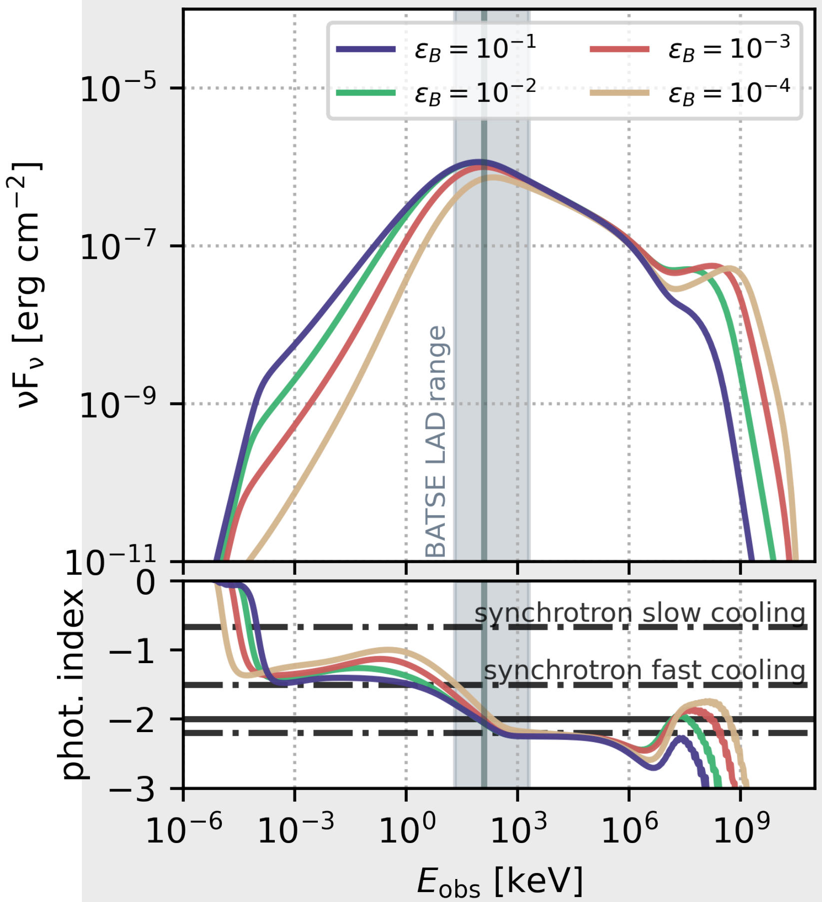

GRB-SP

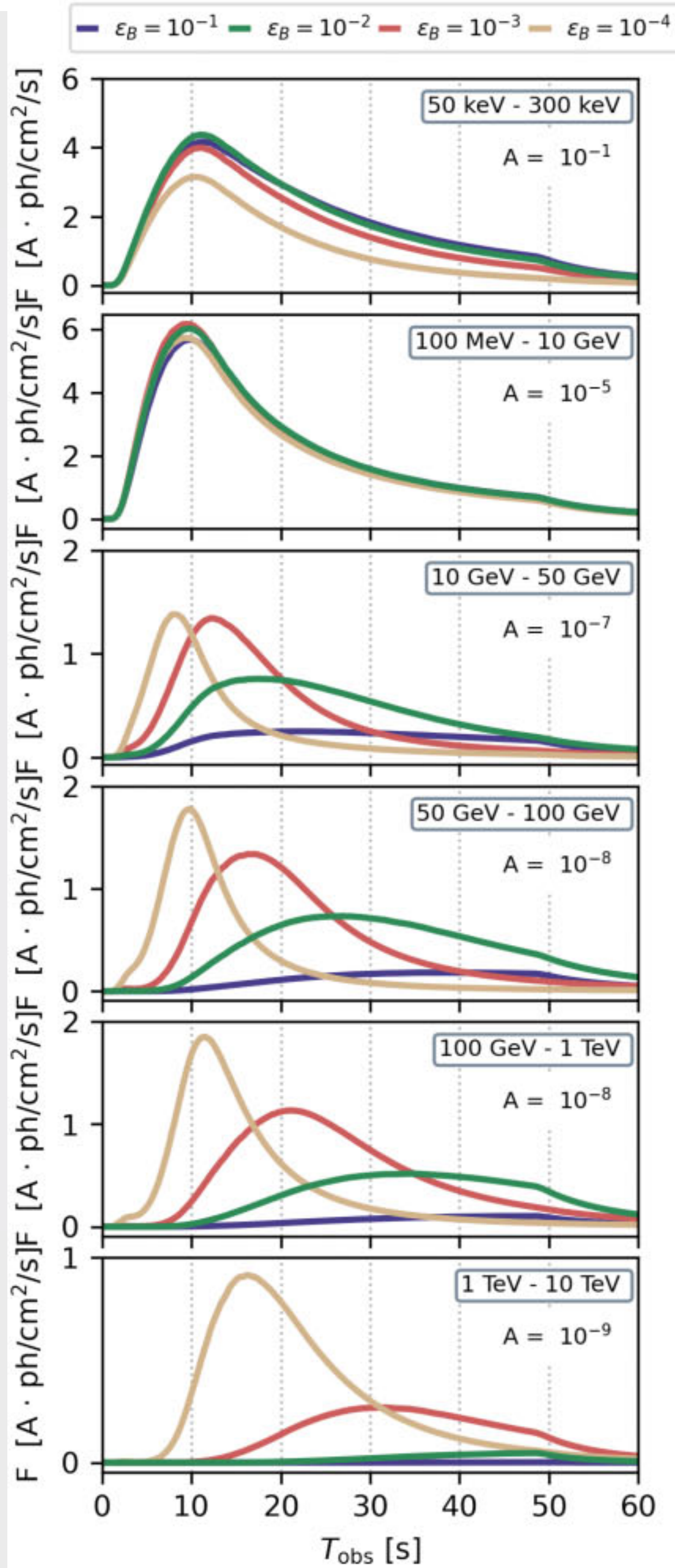

sp-GRB

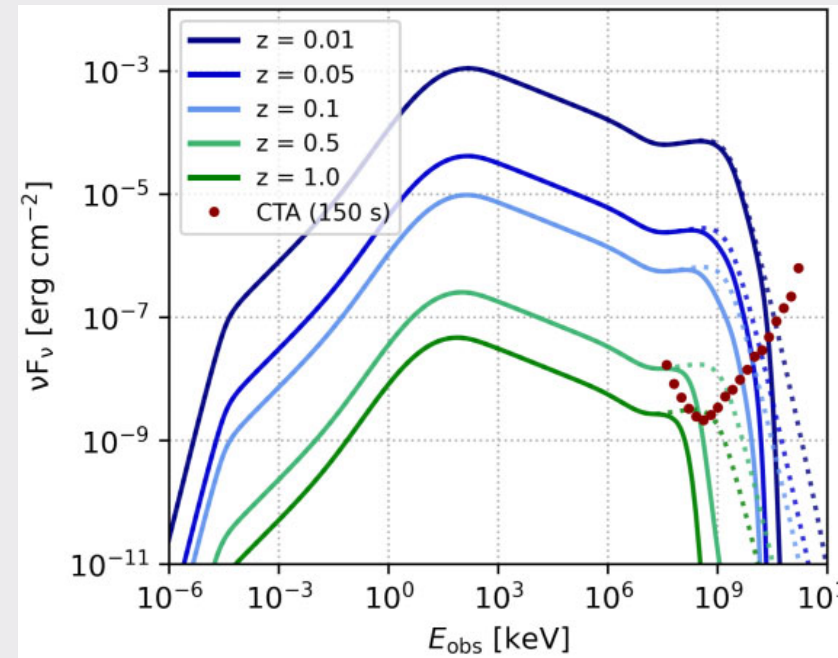

Predicted observed spectra for the prototype hl-GRB with $\epsilon_B = 10^{-3}$ placed at different redshifts.

- minimal fluence detectable by CTA for an observation duration of 150 s.

Rudolph, ŽB, Palladino, Sadeh, Winter 2022

Gao et al 2017 (AM[3])

Maximal energies of cosmic-ray nuclei

The maximal energies are calculated for each collision using the simulated photon spectra and parameters of the jet evolution.

The acceleration rate is balanced with the energy losses (photo-hadronic cooling, photo-disintegration cooling, synchrotron and adiabatic cooling) with NeuCosmA code (Biehl et al 2018).

Iron nuclei (protons) can reach energies up to ≃ 10^{11} GeV (10^{10} GeV).

High ϵ_B yields higher maximal energies.

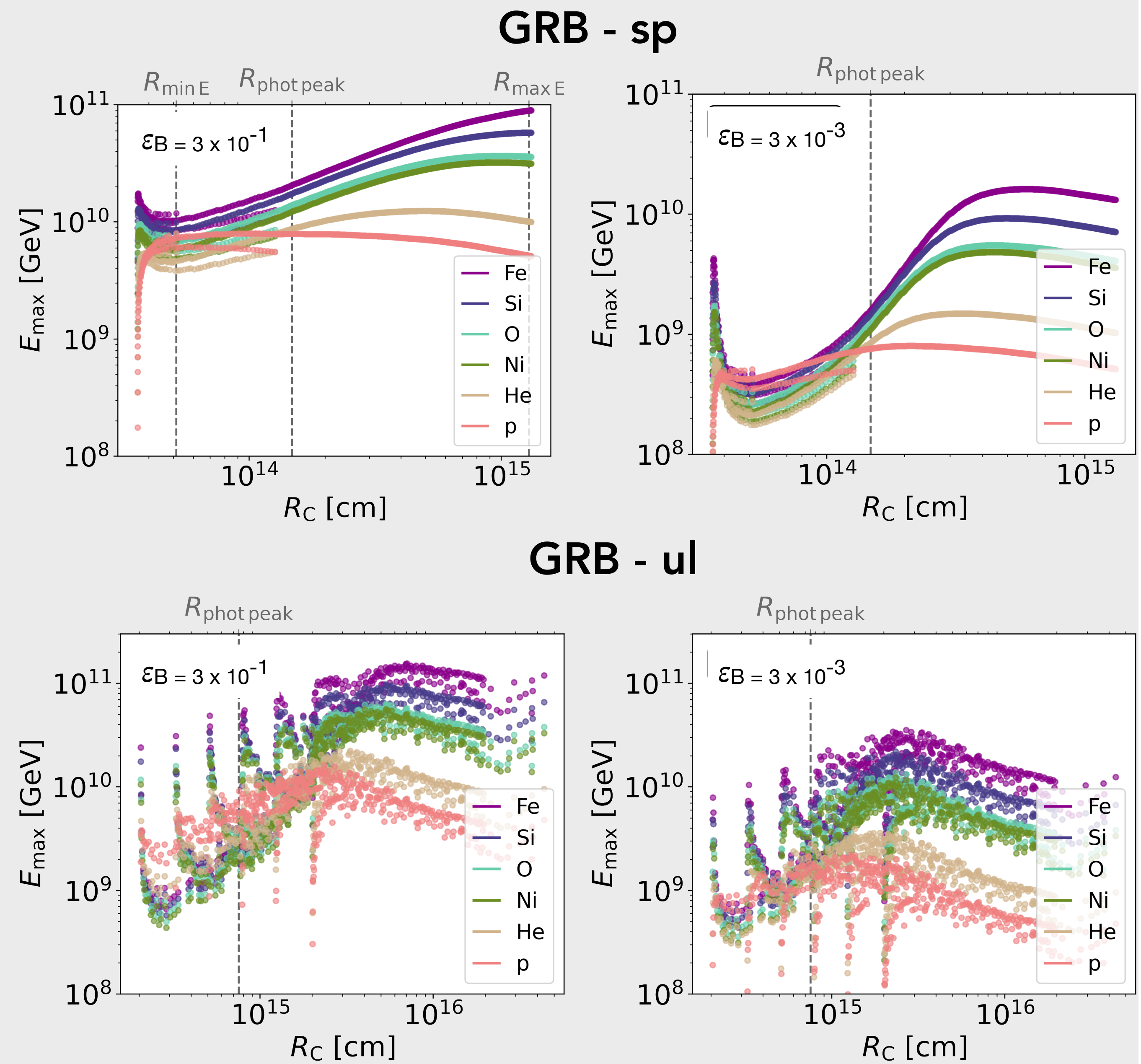

A LL GRB can either have a leptonic inverse Compton VHE component in the photon spectrum (for low ϵ_B) or accelerate cosmic rays to highest energies (for high ϵ_B).

Rudolph, ŽB, Palladino, Sadeh, Winter 2022

Lepto-hadronic model

Rudolph, Petropoulou, ŽB, Winter 2023
Rudolph, Petropoulou, Winter, ŽB 2023

AM[3] time-dependent code (Gao et al. 2017) following the coupled evolution of photons, electrons, positrons, muons, pions, p, n, and ν

All relevant nonthermal processes included: synchrotron emission, SSA, IC scatterings, photopair and photopion production, $\gamma\gamma$-annihilation, adiabatic cooling & escape

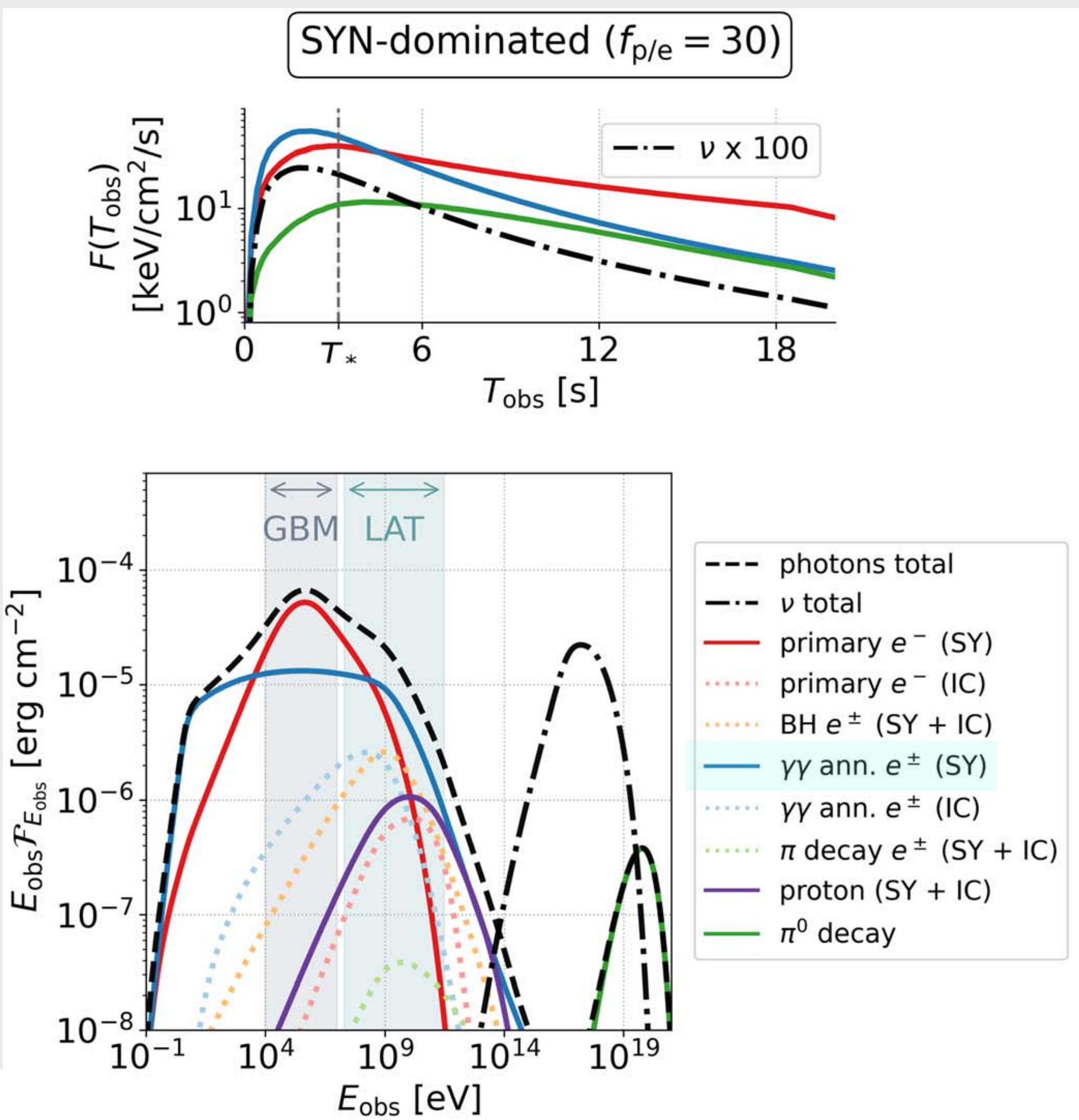

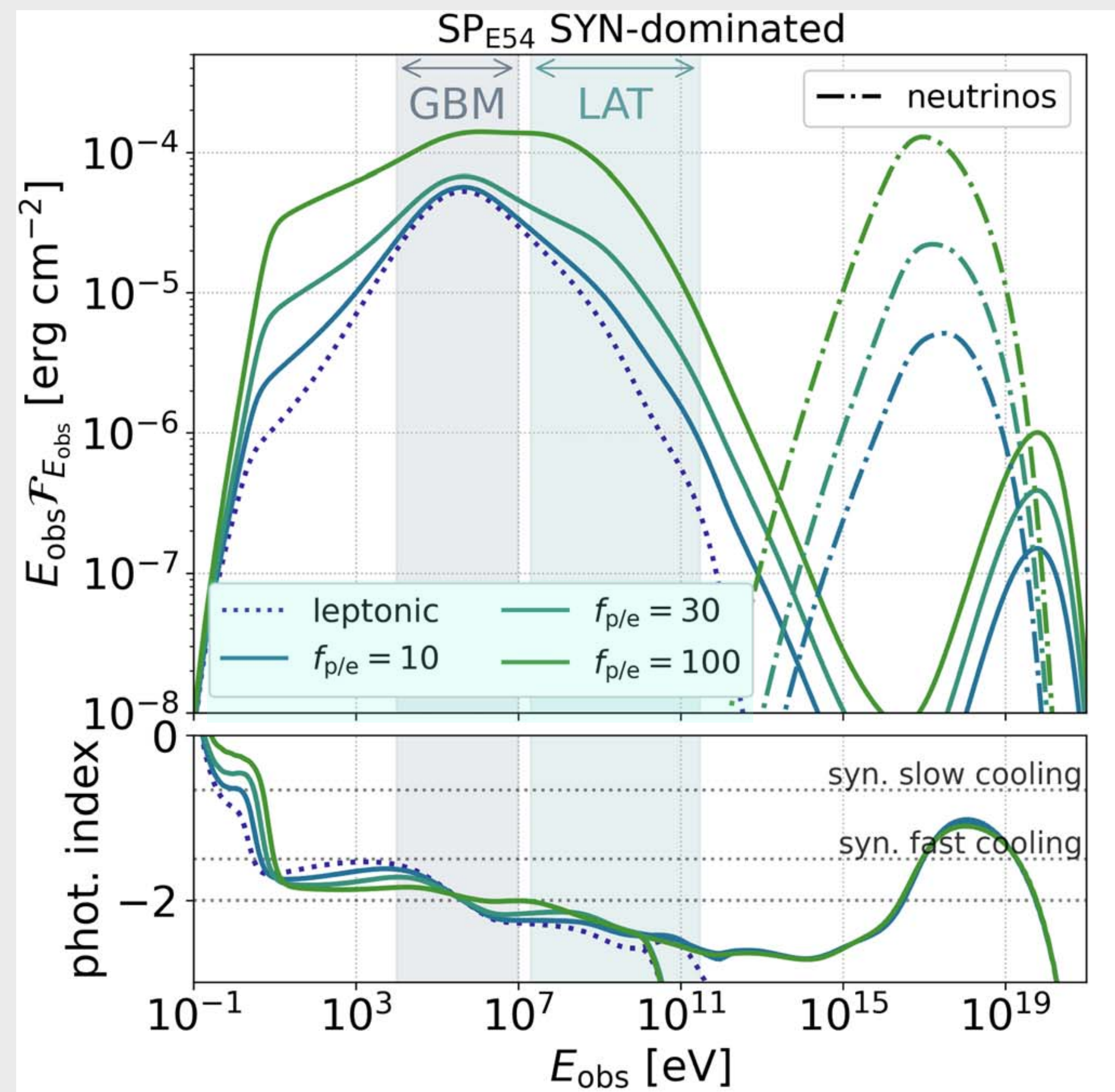

GRB 221009A

Locations of the dust layers associated with the five smallest X-ray rings from the GRB 221009A:

- GRB occurred at low Galactic latitude

The direction to the burst; dark patches represent the dust layers responsible for producing the X-ray rings

- the smallest ring corresponds to the most distant dust

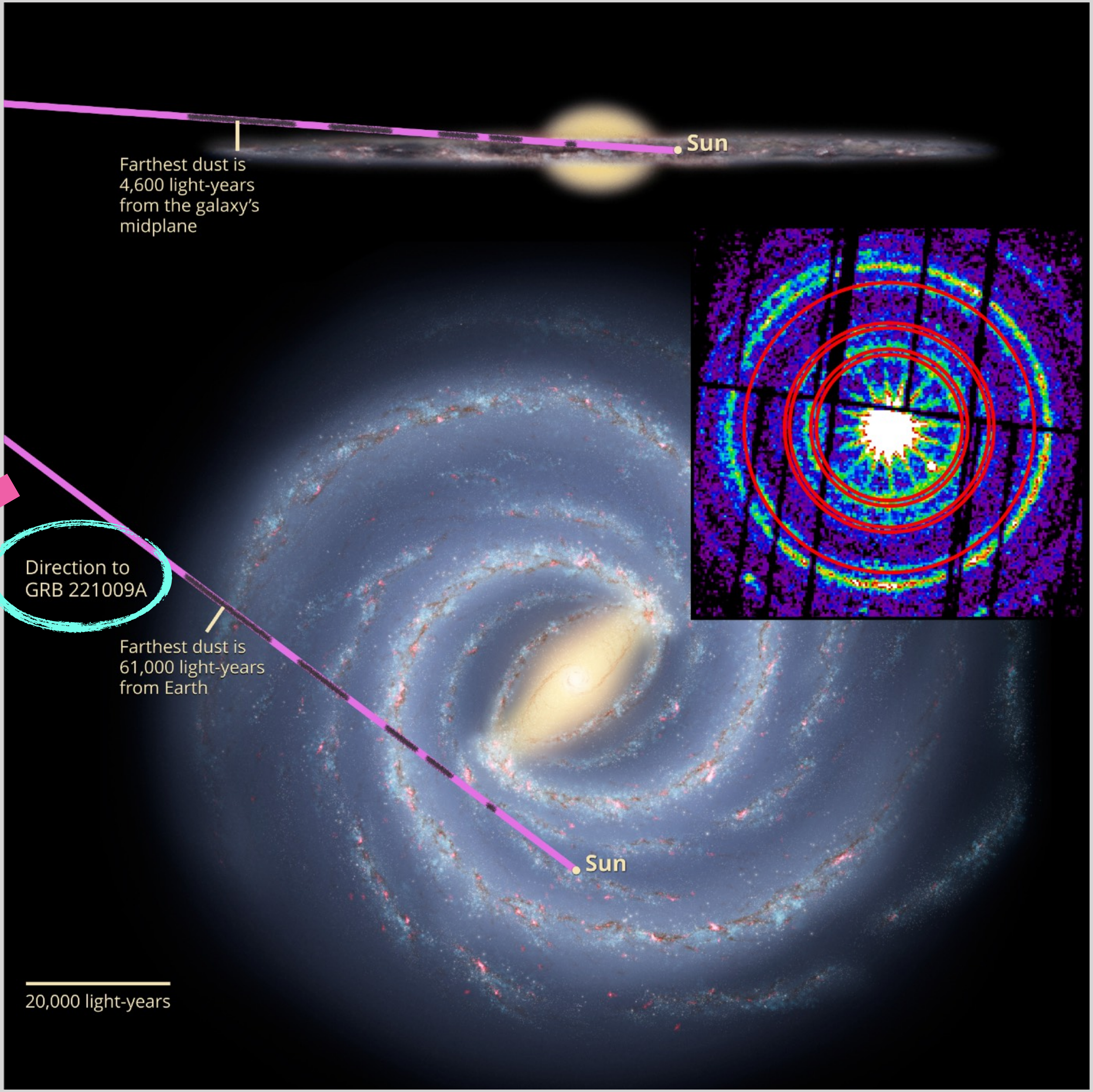

Credit: NASA's Goddard Space Flight Center

Dust scattered X-ray halos around GRBs

Dust scattered X-rays detected at off-axis angle θ ($\approx \theta_{sca}$ if $d_{dust} << d_{source}$) will have a time delay:

$$t - t_0 = \frac{x}{1-x}\frac{d_{source}\theta^2}{2c}$$

$$\theta(t) = \sqrt{\frac{1-x}{x}\frac{2c(t-t_0)}{d_{source}}} \approx \sqrt{\frac{2c(t-t_0)}{d_{dust}}} \quad \text{if } d_{dust} << d_{source}$$

Halo photons scattered at larger radii suffer greater time delay owing to their longer paths.

A. Tiengo

GRB 221009A

GRB 221009A: EPIC 0.7-4 keV images [counts/s/arcmin²] of the expanding rings

The two red circles of radii 8′ and 11′ : a reference for ring expansion.

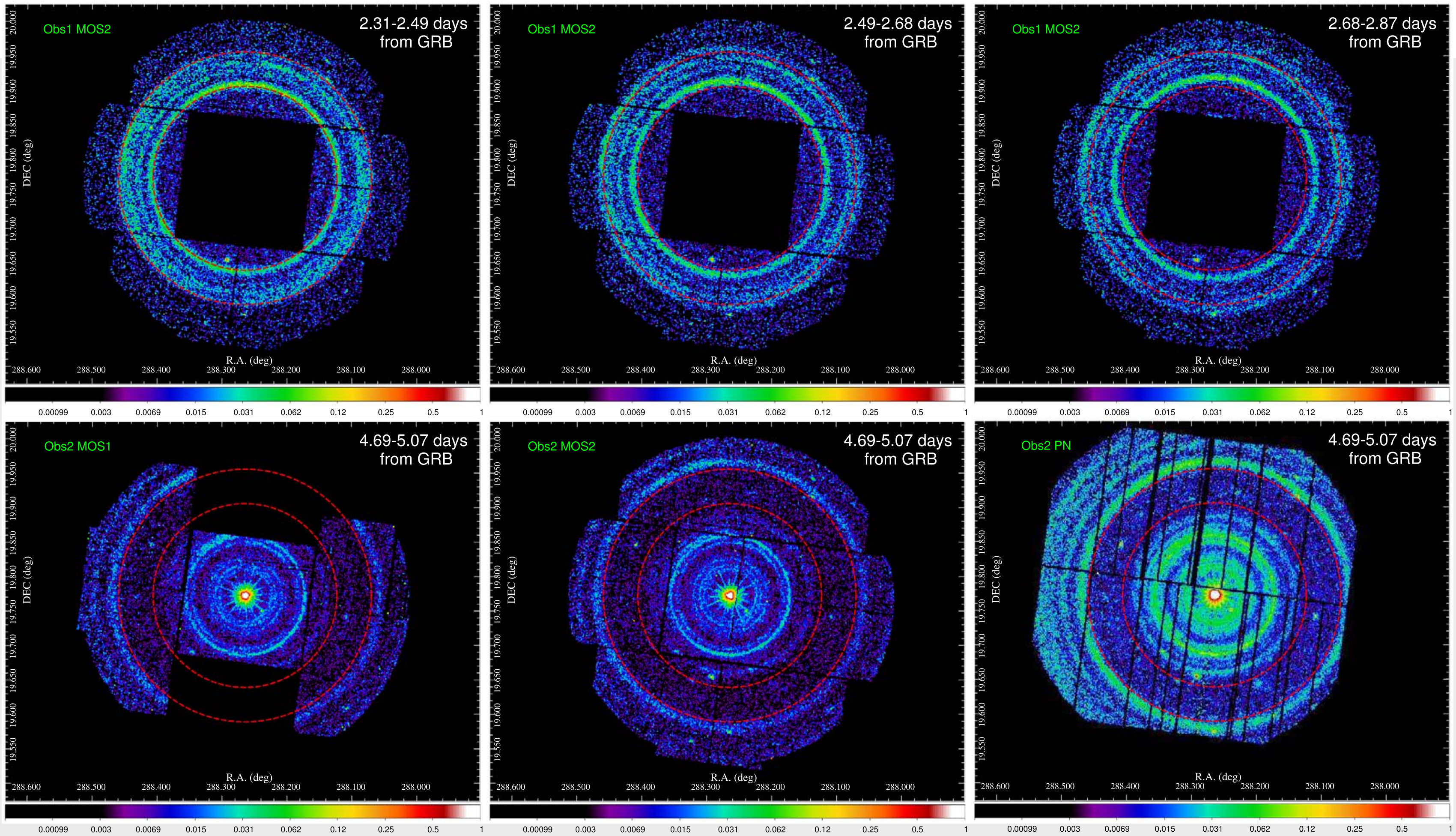

Tiengo, Pintore, ..ŽB, Jelić, Campana 2023
Šiljeg, ŽB, Jelić, Tiengo et al. 2023
Vaia, ŽB et al. 2025

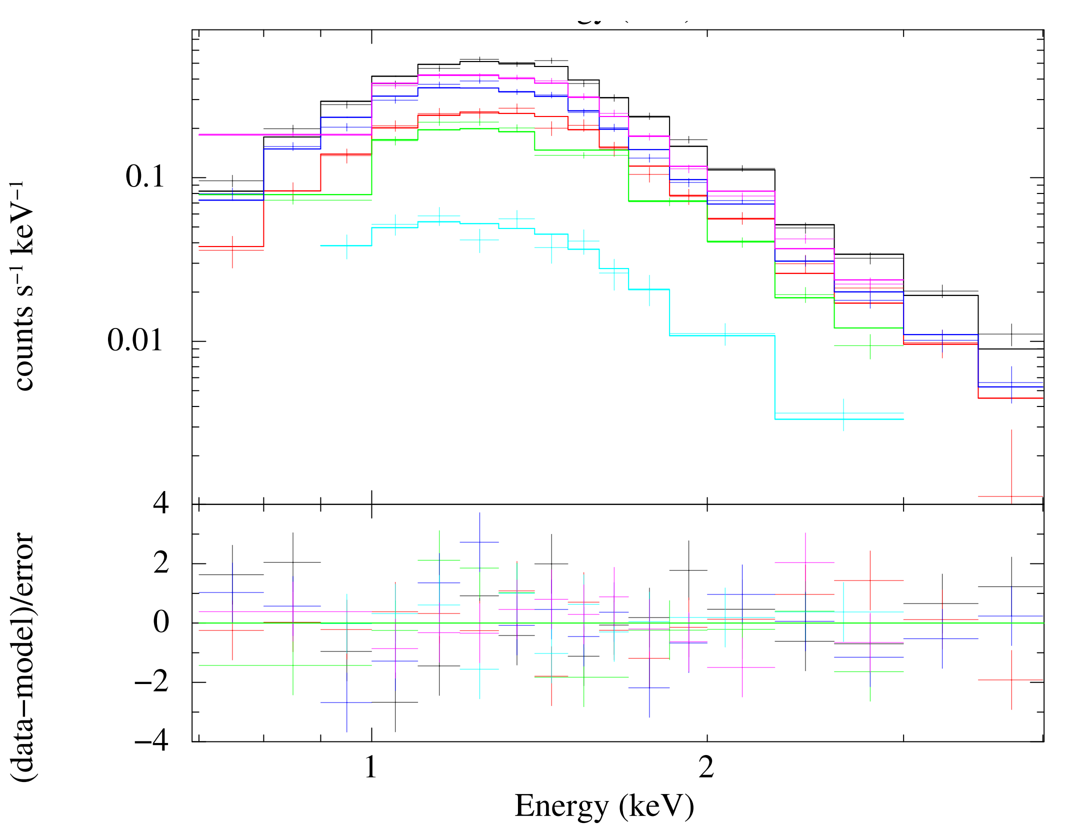

MOS2 spectra of rings 1-6 (Tiengo et al. 2023)

By fitting the spectra of the rings with different models for the dust composition and grain size distribution —> the spectrum of the GRB prompt emission in the 0.7 - 4 keV as an absoprbed power law with photon index **Γ** =1 -1.4

The photon index and the fluence indicate the presence of a possible soft excess with respect to the extrapolation of the main GRB peak!

‣ **Comparison of distance measurements to dust clouds using GRB x-ray halos and 3D dust extinction**

Šiljeg, ŽB, Jelić, Tiengo et al. MNRAS 2023

We used four 3D extinction maps that exploit photometric data from different surveys and apply diverse algorithms for the 3D mapping of extinction
→ we compared the X-ray halo derived distances with the local maxima in the extinction density distribution.

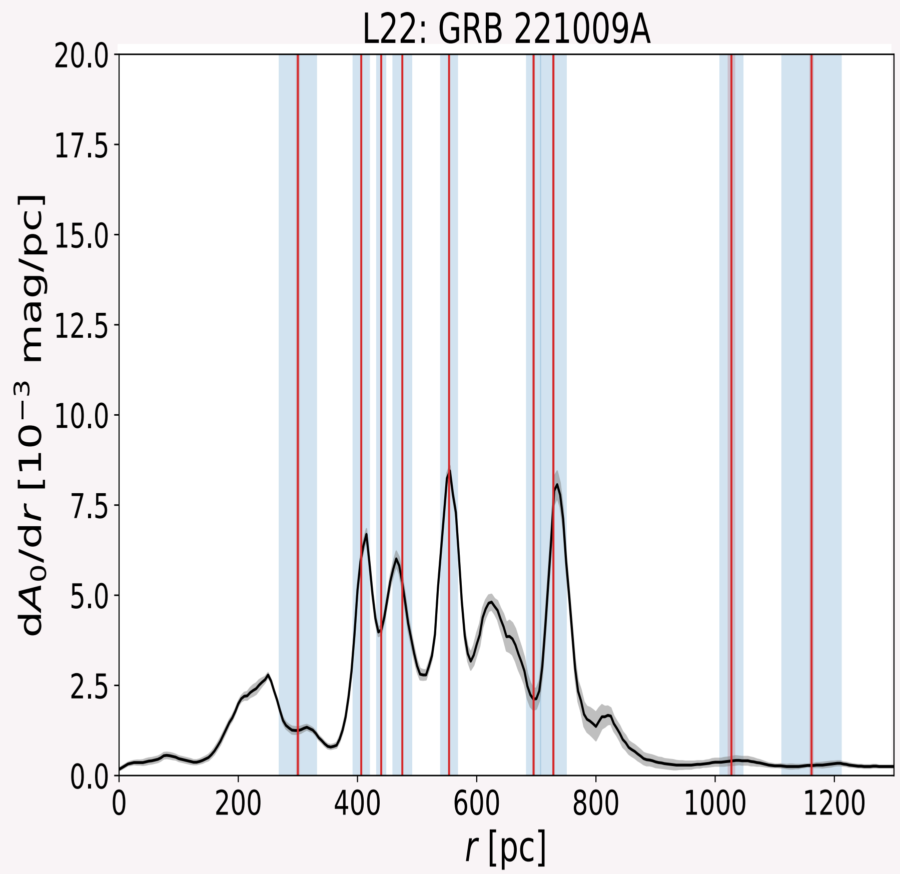

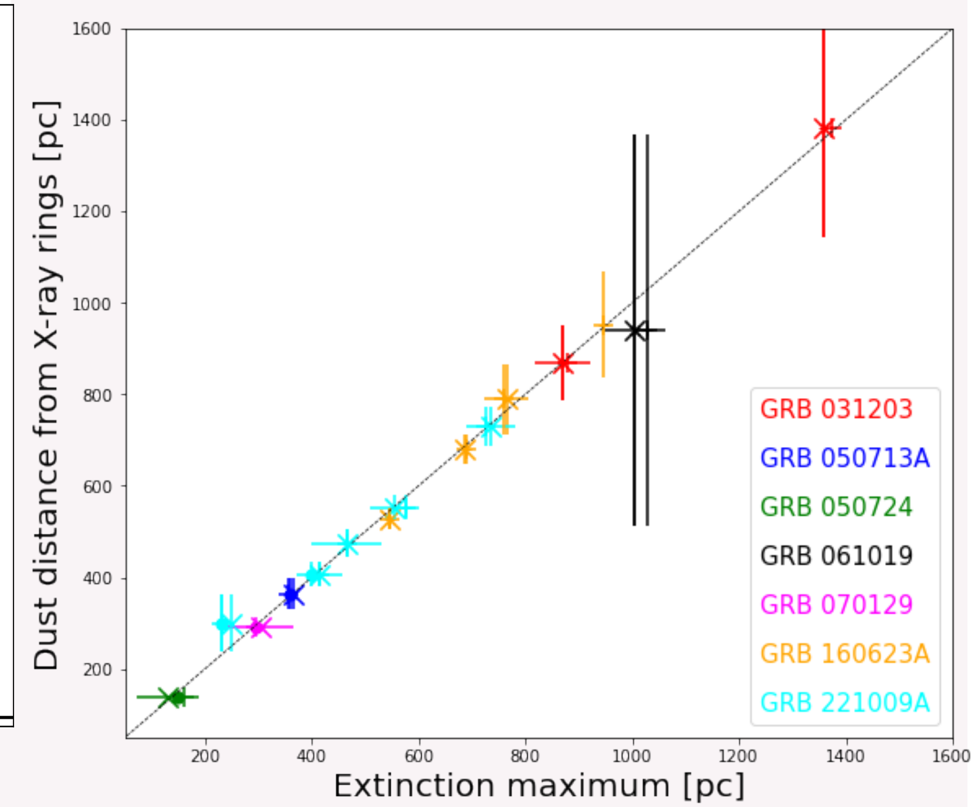

2D cut of extinction density cube from L22 map perpendicular to the plane of the galaxy in the direction of GRB 221009A. Height is measured with respect to the position of the plane of galaxy:

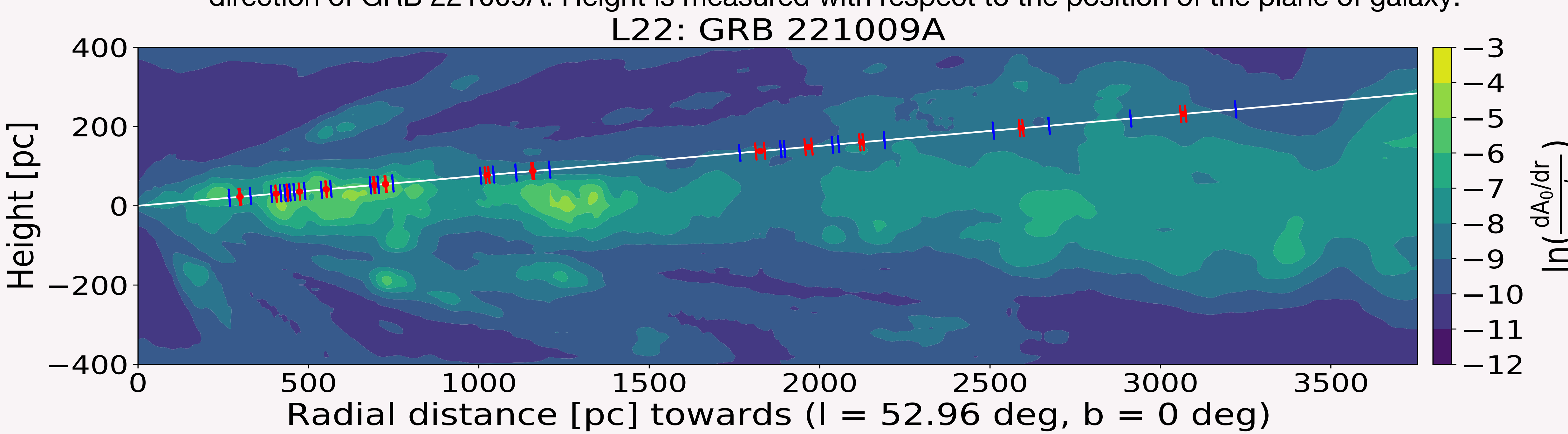

GRB prompt emission from the synchrotron radiation of relativistic electrons in a decaying magnetic field

Daigne & Bosnjak 2025

▸ Motivation

The theoretically predicted synchrotron spectrum leads to a slope $F_\nu \propto \nu^{-1/2}$ below 100 keV, which is in contradiction to the much harder spectra observed during the prompt GRB emission.

Sari, Piran & Narayan 1998

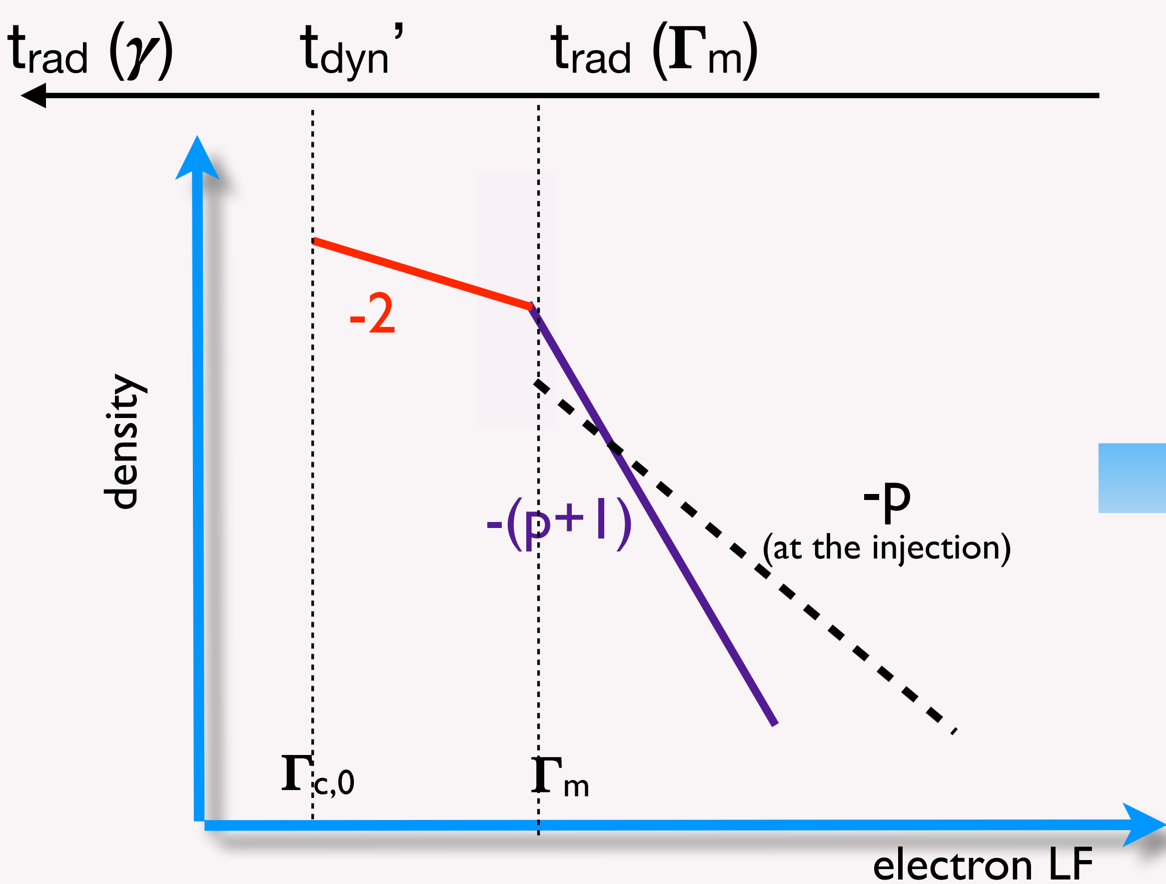

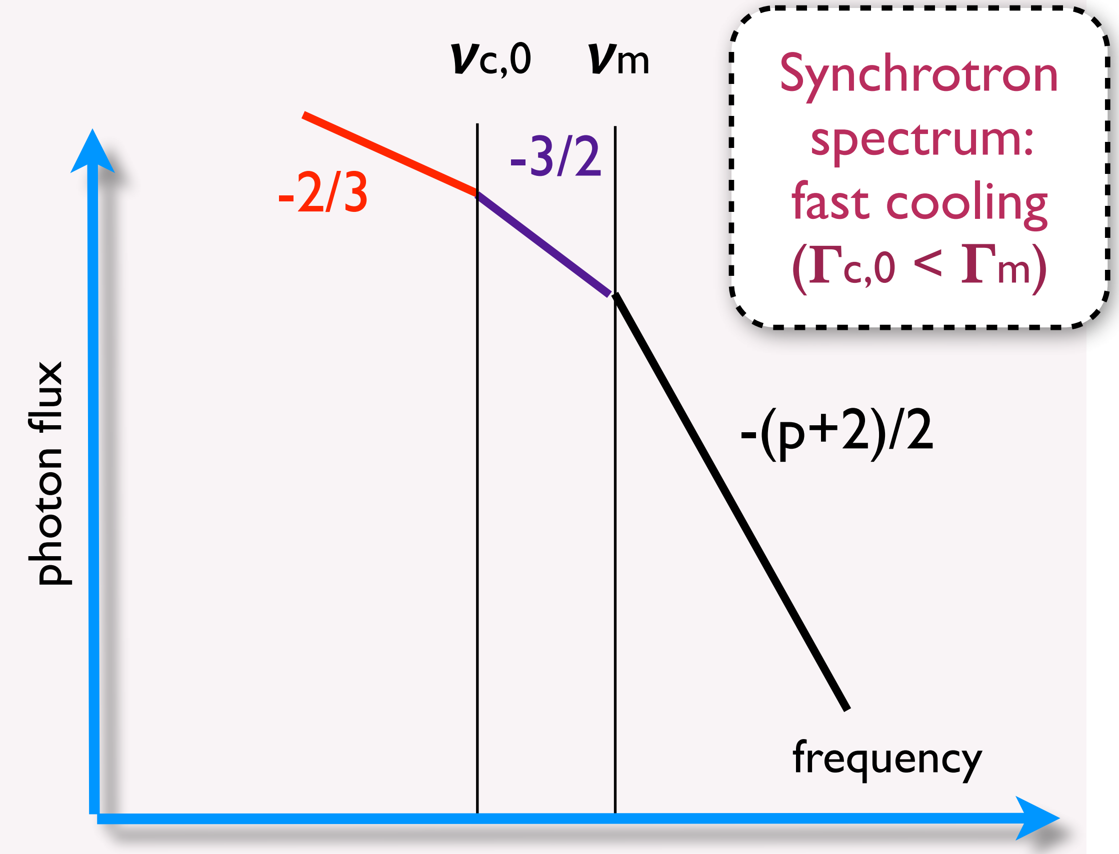

Γ_m: minimum Lorentz factor at injection

$\Gamma_{c,0}$: radiative timescale = dynamical timescale

A possible solution proposed by Daigne et al. 2011; Beniamini & Piran 2013: in **the marginally fast cooling regime** ($\Gamma_{c,0} \simeq (0.1 - 1)\, \Gamma_m$), where the cooling break is very close to the peak frequency, the intermediate portion of the spectrum (slope = -3/2) disappears and the slope -2/3 is recovered (still with a high radiative efficiency)

GRB prompt emission from the synchrotron radiation of relativistic electrons in a decaying magnetic field

- **Motivation**

Marginally fast cooling can naturally emerge if electrons are radiating in a magnetic field decaying on a timescale t_B',

$$\boxed{B'(t') = B_0' \, e^{-t'/t'_B} \quad \text{where} \quad t'_{syn}(\Gamma_m) < t'_B < t'_{dyn}}$$

→ electrons having $\gamma \gtrsim \Gamma_m$ will still experience a magnetic field B'_0 and the peak + high-enegy part of the synchrotron spectrum will not be affected

→ electrons with Lorentz factors $\Gamma_{c,0} < \gamma < \Gamma_m$ will lose their energy more slowly than expected because they will encounter a lower magnetic field when they start to travel outside the initial acceleration site. The cooling break will increase to:

$$\nu_c \simeq \nu_{c,0} \, (t'_{dyn} / t'_B)^2$$

This allows to naturally tend towards the marginally fast cooling regime, even when $\Gamma_{c,0} / \Gamma_m << 1$. The radiative efficiency will remain high as long as $t'_{syn}(\Gamma_m) << t'_B$ so the final condition becomes:

$$\boxed{\Gamma_{c,0} / \Gamma_m \lesssim t'_B / t'_{dyn} \lesssim 1}$$

Radiative models

A hierarchy of scales: $t'_{acc}\,(\boldsymbol{\Gamma}_m) \ll t'_{rad}\,(\boldsymbol{\Gamma}_m) \ll t_{dyn}'$

- the magnetic field may decay on a length scale much shorter than the shocked region scale t'_{dyn} (e.g. Keshet et al. 2009).

Radiating electrons probe the magnetic field on >> scale than in the PIC simulations but - when they are in fast cooling - on a much smaller scale than the (magneto-) hydrodynamical scale.

Prompt emission models: Pe'er & Zhang 2006; Derishev 2007; Zhao et al. 2014; Uhm & Zhang 2014; Geng et al. 2018 (much larger scales for B' decay)

Afterglow modelling: Gruzinov 2001; Rossi & Rees 2003; Lemoine 2013

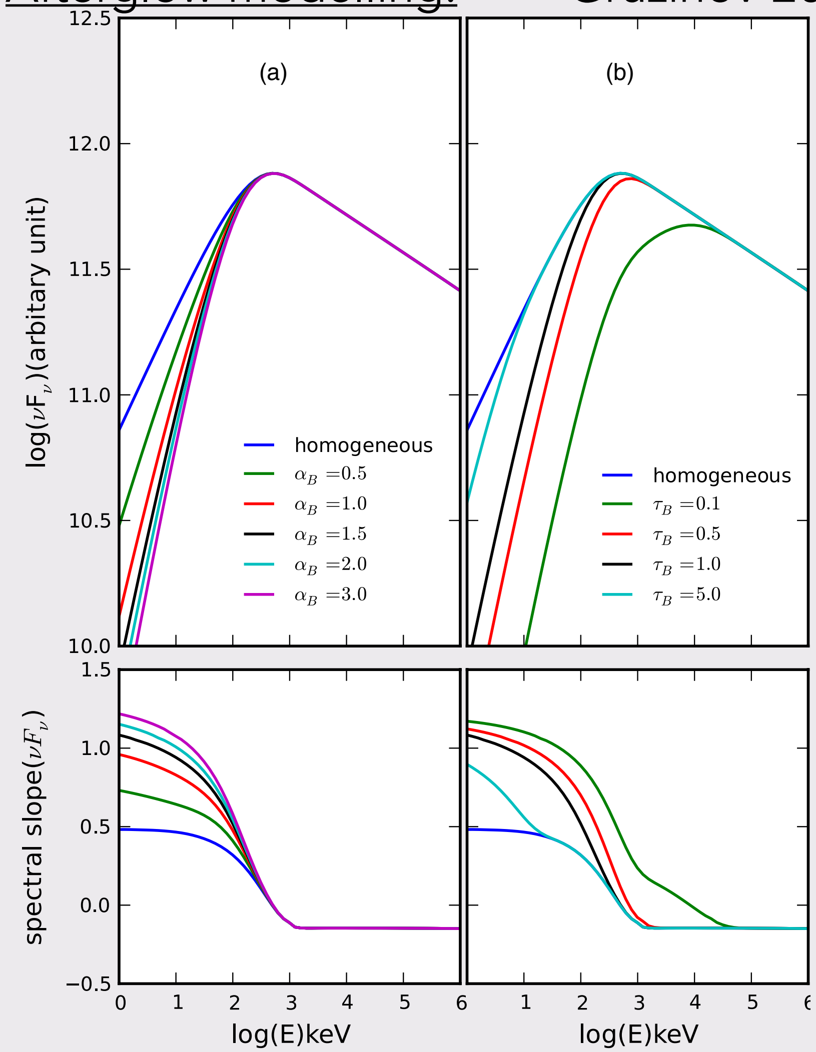

Zhao et al. 2014:

PLD & ED models

Klein-Nishina effects neglected

adiabatic cooling not included

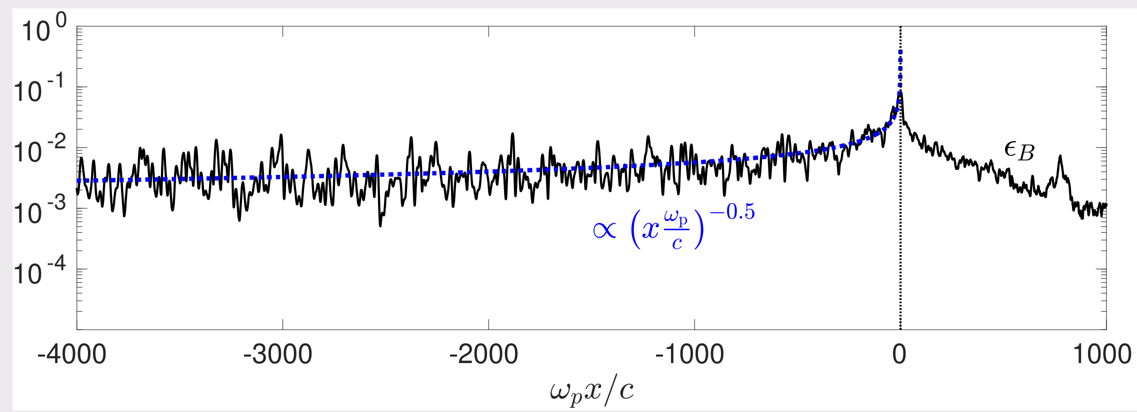

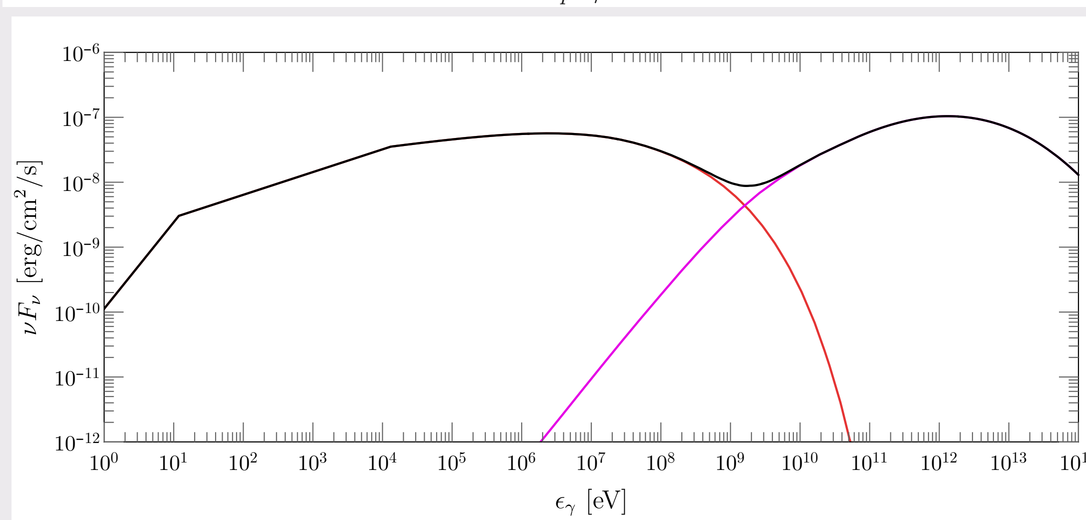

$\epsilon_B = 0.01$ in the shock vicinity
$\epsilon_B \propto (x\,\omega_p / c)^{-0.4}$
$E = 8 \times 10^{53}$ erg
$z = 0.4$
$n = 0.03$ cm^{-3}
$\epsilon_e = 0.1$
$s = 2.3$
$\gamma_{e,\,max} = 2 \times 10^7$

Vanthieghem et al. 2020:

- decay of the microturbulence in the shocked region $\epsilon_B \propto (x\,\omega_p/c)^{-0.5}$
- all electrons (but those of the very highest energies) cool in a region in which the turbulence has decayed

Radiative model: exponential decay of the magnetic field

- The magnetic field decay: $B'(t') = B_0' \, e^{-t'/t_B'}$

Electrons radiate efficiently only above an effective Lorentz factor:

$$\Gamma_{c,\mathrm{eff}} \simeq \Gamma_{c,0} \, (t'_{\mathrm{dyn}} / t'_B)$$

which leads to an increase of the cooling break frequency by a factor $\mathbf{(t_{dyn}'/t_B')^2}$

For an extreme decay, we expect a slow cooling spectrum even for $\Gamma_m > \Gamma_{c,0}$

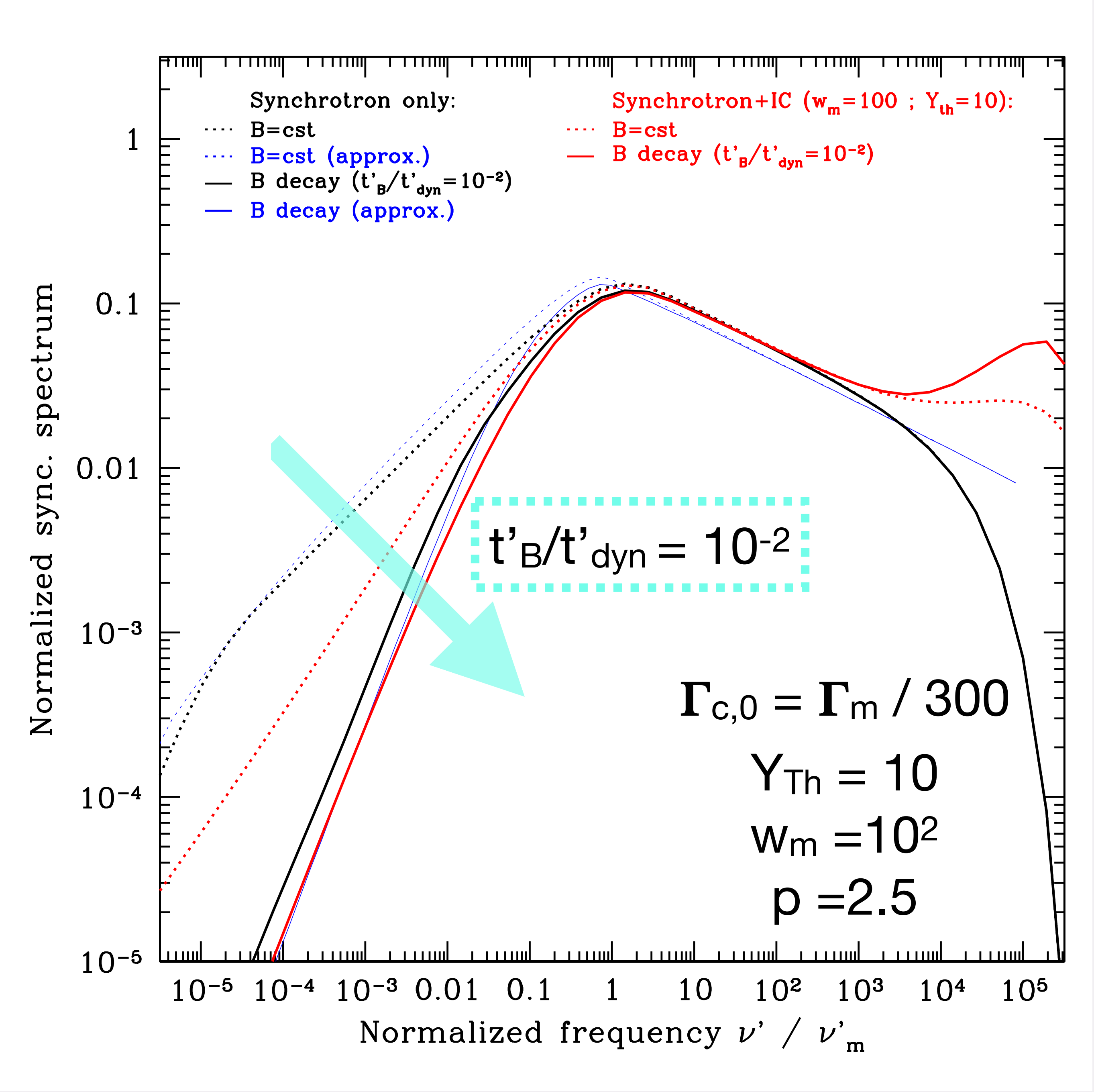

Daigne & Bošnjak 2025

Effect of $Y_{Th,0}$ and w_m which govern the importance of inverse Compton scatterings and of Klein-Nishina corrections:

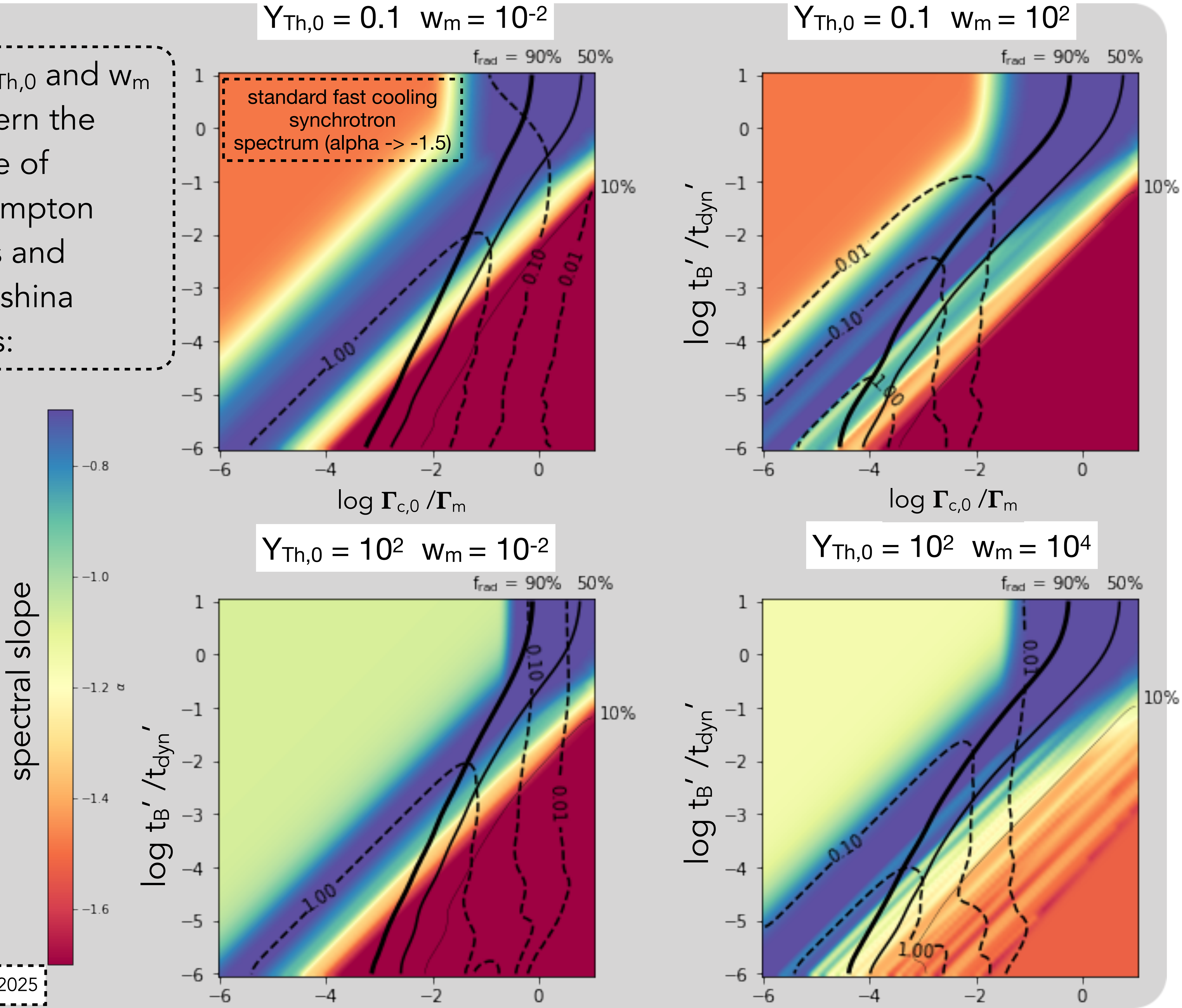

Daigne & Bošnjak 2025

Spectral evolution in the internal shock model: steep low energy slopes

Case B: a single pulse burst with a low magnetic field. The main spectral peak is due to synchrotron emission (Bošnjak, Daigne & Dubus 2009)

$\epsilon_B = 5 \times 10^{-3}$, $\epsilon_e = 1/3$, $\xi = 2 \times 10^{-3}$, $p = 2.5$, $dE/dt = 5 \times 10^{53}$ erg/s

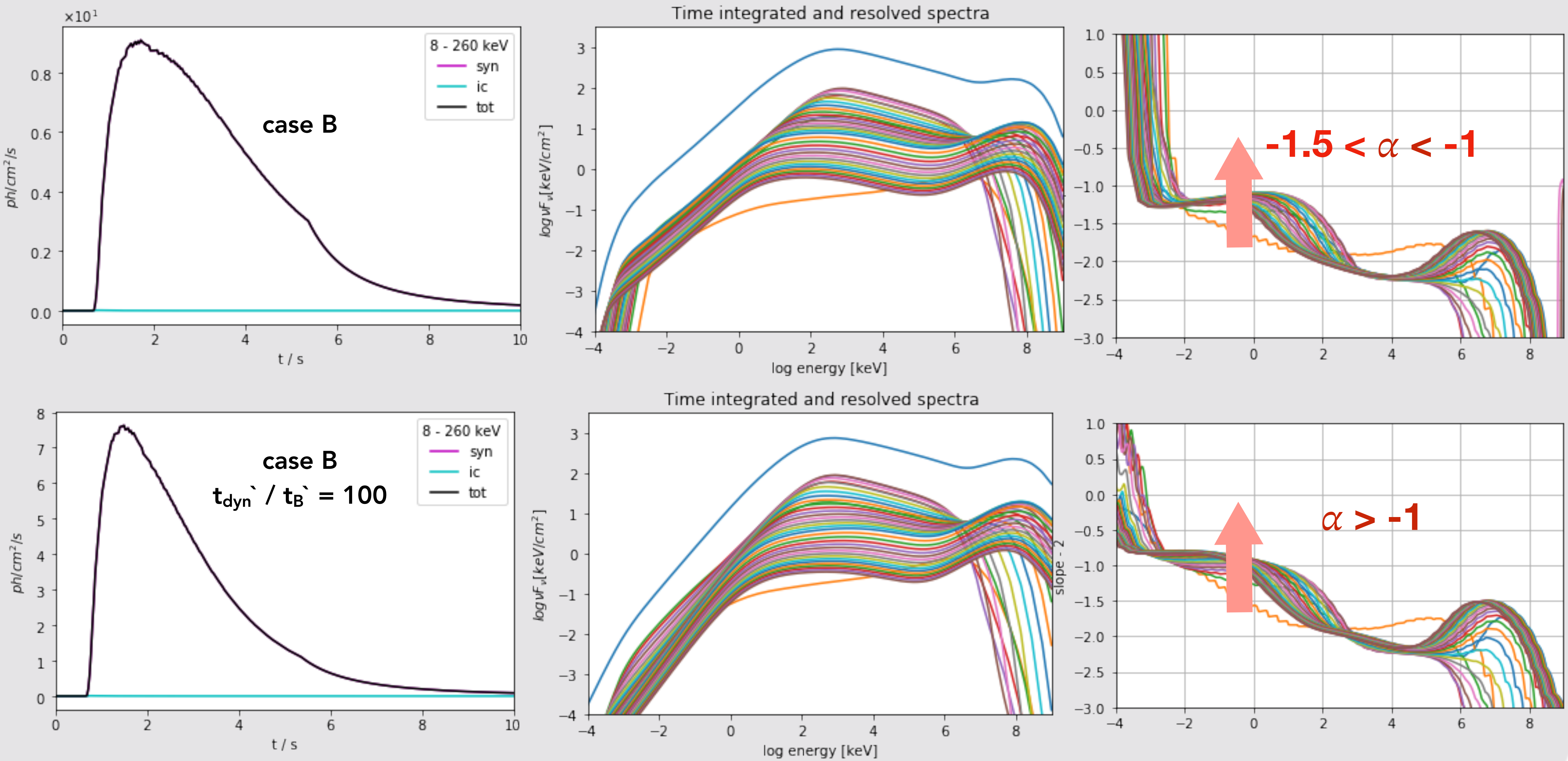

Effect of a decaying magnetic field in the internal shock model: reference case B with $t_B/t_{dyn} = 10^{-3}$:

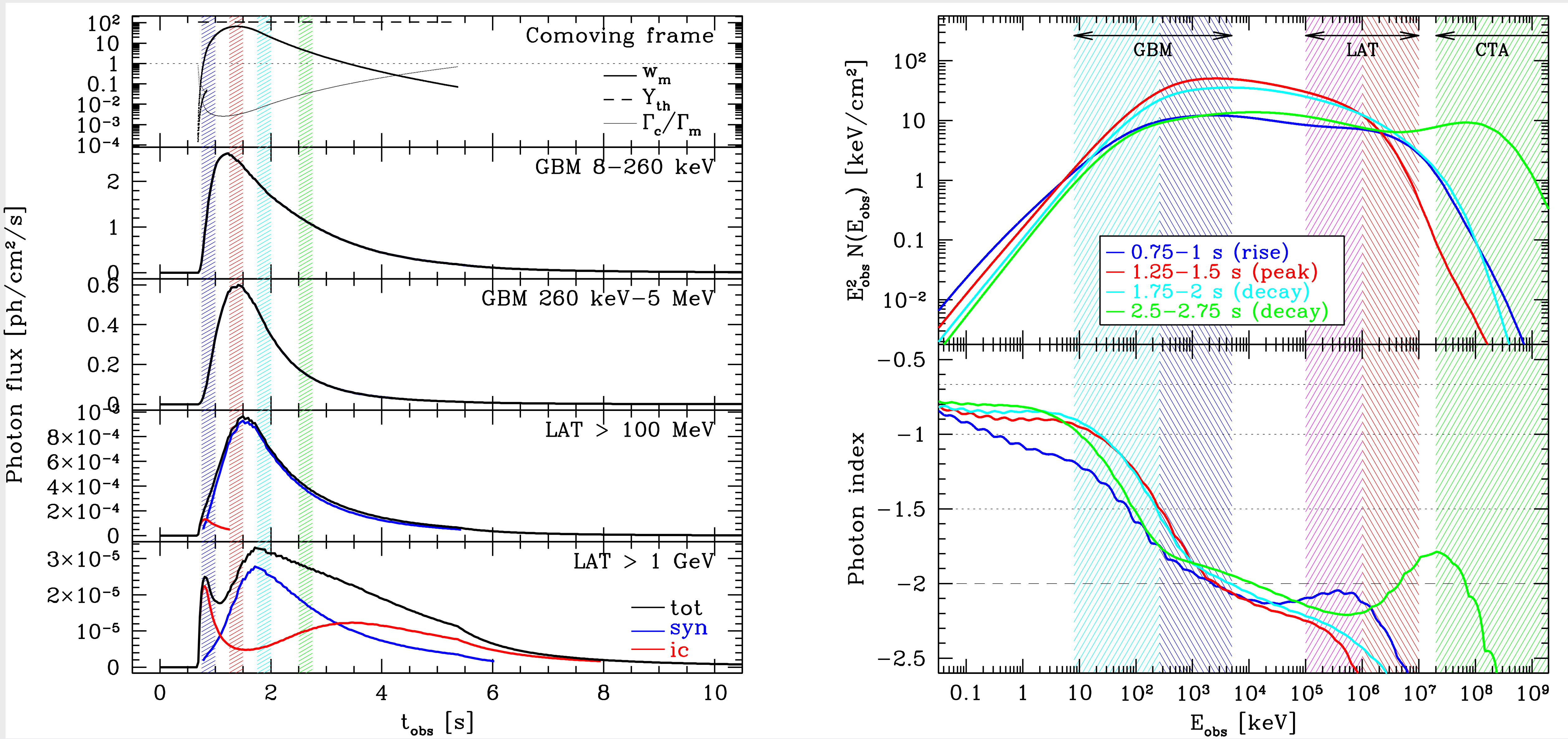

Daigne & Bošnjak 2025

Off-axis MeV and very-high energy gamma-ray emissions from structured gamma-ray burst jets

ŽB, Zhang, Murase, Ioka 2024

‣ Motivation

Ioka & Nakamura (2018) considered that sGRB 170817A is faint because the jet is off-axis to our line of sight (Abbott et al. 2017; Granot et al. 2017; Lamb & Kobayashi 2018)

Most of the emission is beamed into the on-axis direction via a relativistic effect and an off-axis observer receives photons emitted outside the beaming cone → the apparent energy of the off axis jet becomes faint (Ioka & Nakamura 2001; Yamazaki et al. 2018)

EM counterparts associated with binary NS merger have been anticipated:

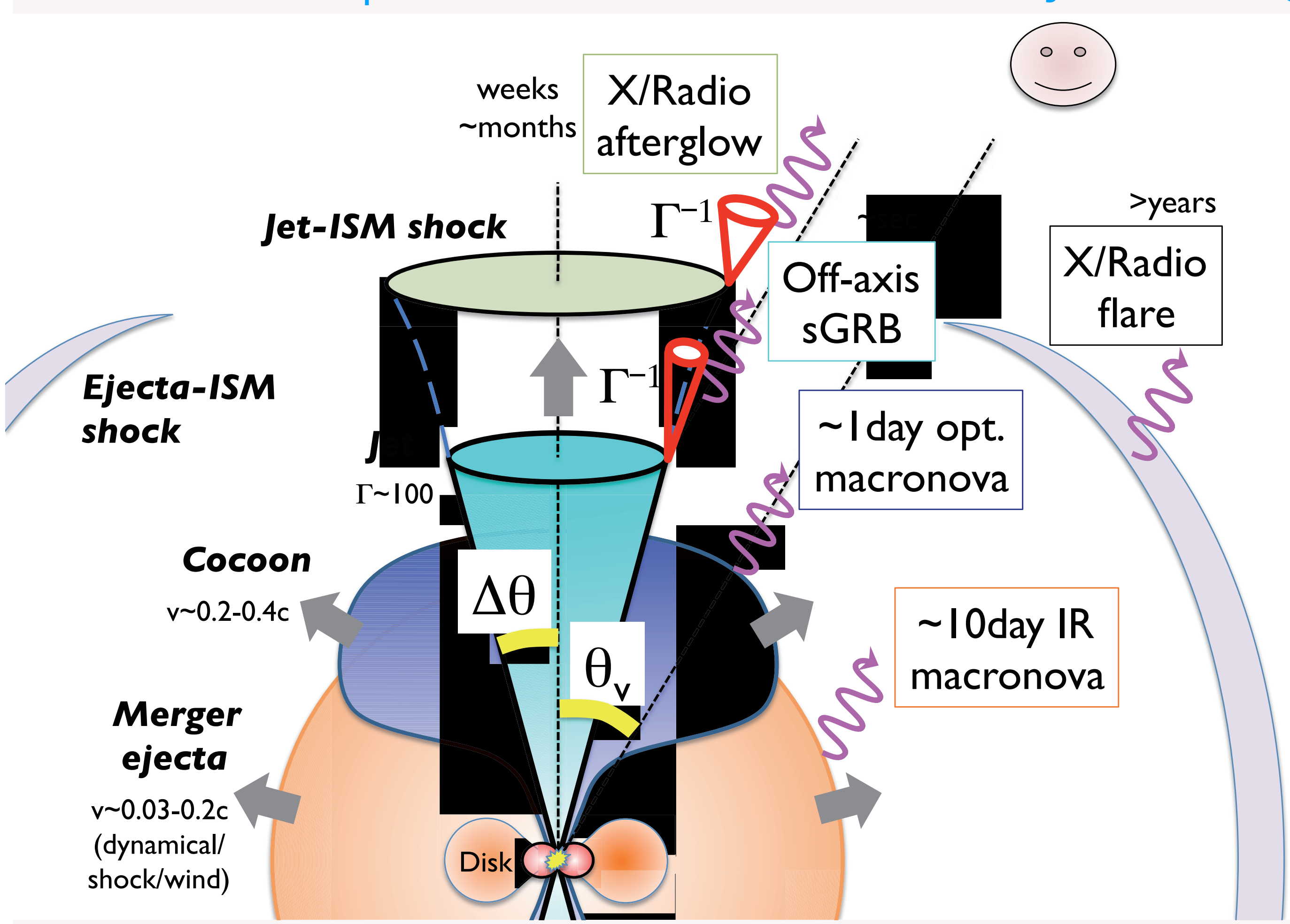

Ioka & Nakamura 2018

1. a binary NS merger is at the origin of sGRB
2. sGRB produces an afterglow via interaction with the interstellar medium. For off-axis observers, the early afterglow looks faint
3. a small amount of NS material ejected from the NS merger is expected to emit optical-IR signal ('macronova')
4. a radio flare and the associated X-ray remnants occur through the interaction between the merger ejecta and the ISM

Off-axis MeV and very-high energy gamma-ray emissions from structured gamma-ray burst jets

- **Motivation**

The off-axis model was initially studied by using a top-hat jet with uniform brightness and a sharp edge → the simplest off-axis model seems to be difficult to explain $\nu_{\rm peak}$ ~185 keV

The afterglow observations including VLBI observations of superluminal motion revealed a jet with $E_{\rm iso} > 10^{52}$ erg, a narrow core $\theta_c \lesssim 5^\circ$ and a viewing angle ~ 14° - 28° (Mooley et al. 2018; Ghirlanda et al. 2018)

Ioka & Nakamura 2019: the central part should be much more energetic than the observed sGRB 170817A

$$\boxed{E_\gamma(\theta) = \epsilon_\gamma E_0 \exp(-\theta^2/2\theta_c^2)}$$

$E_0 = 10^{52.8}$ erg

$\theta_c = 0.059$

$n = 10^{-2.51}$ cm^{-3}

$\theta_v = 0.38 \approx 22^\circ$

Troja et al. 2018

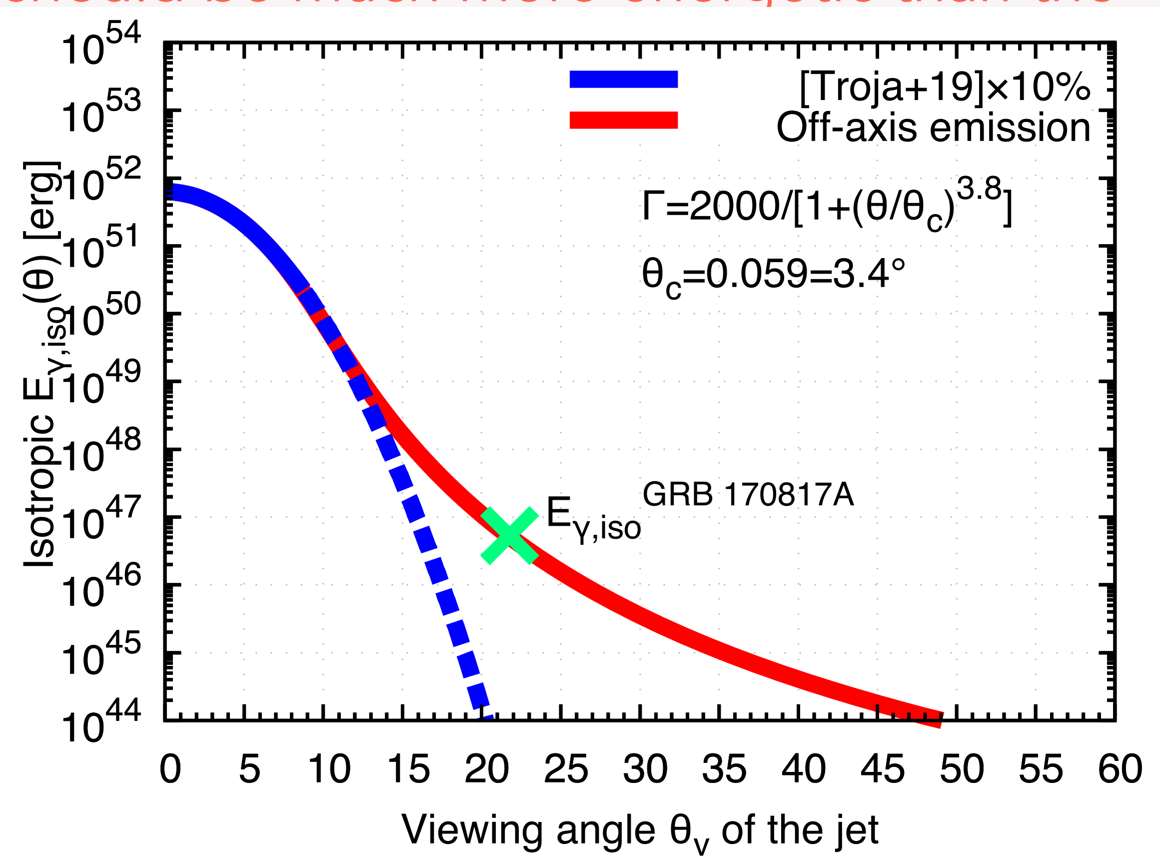

‣ Off-axis emission from a structured jet

The surface brightness
(the isotropic energy per solid angle):

$$\frac{\mathrm{d}E_{\gamma,\mathrm{iso}}}{\mathrm{d}\Omega} = \frac{1}{4\pi}\frac{E_\gamma(\theta)}{\Gamma^4(1-\beta\cos\theta_\Delta)^3}$$

$$\cos\theta_\Delta = \sin\theta\cos\phi\sin\theta_v + \cos\theta\cos\theta_v$$

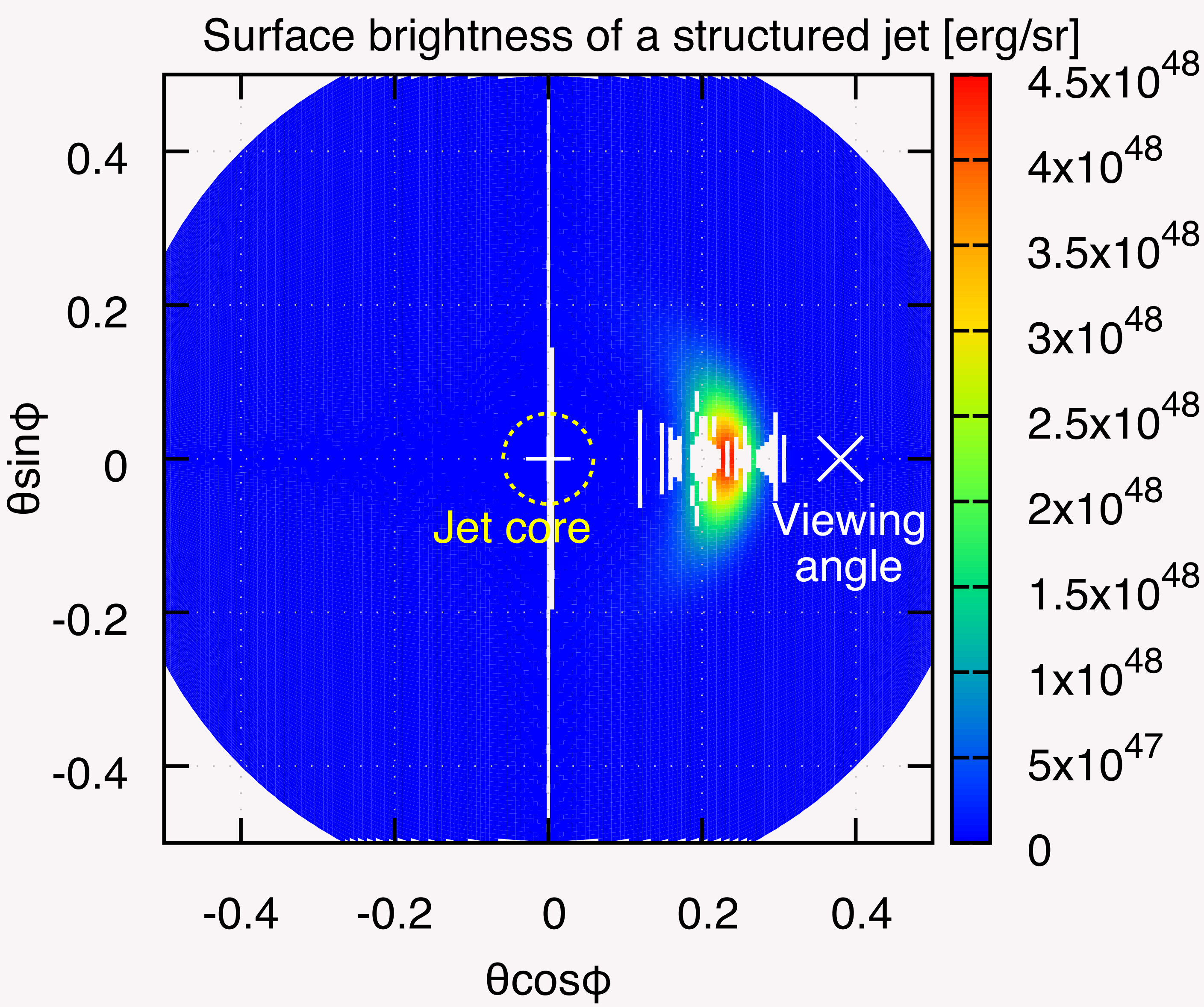

Ioka & Nakamura 2019

The off-axis model for GRB 170817A predicted that the most luminous region arises neither from the jet core, nor at the line of sight at the viewing angle, but from the off-centre jet.

Off-axis MeV and very-high energy gamma-ray emissions from structured gamma-ray burst jets

ŽB, Zhang, Murase, Ioka 2024

- **TeV photons**

The different energy photons (MeV, TeV) arrive to the observer from different emission zones for off-axis structured jets, mainly due to the effect of the two-photon pair annihilation process

The optical depth for VHE photons is much higher in the core region near the jet surface, which gradually decreases outwards allowing VHE photons to escape.

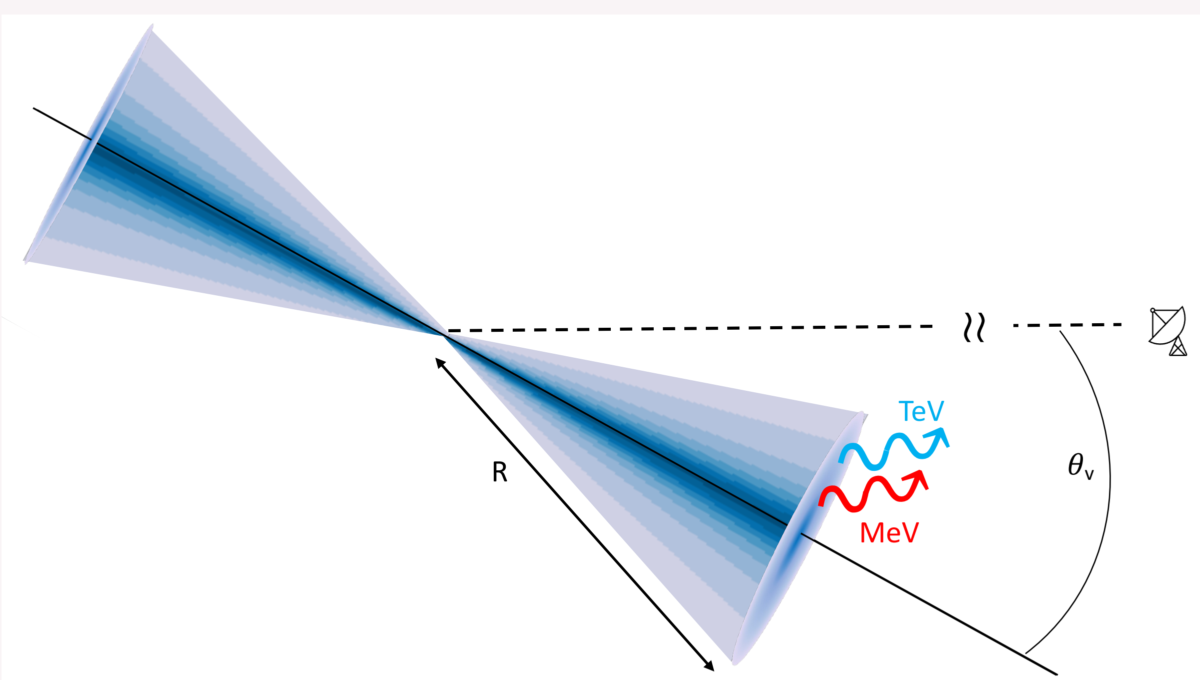

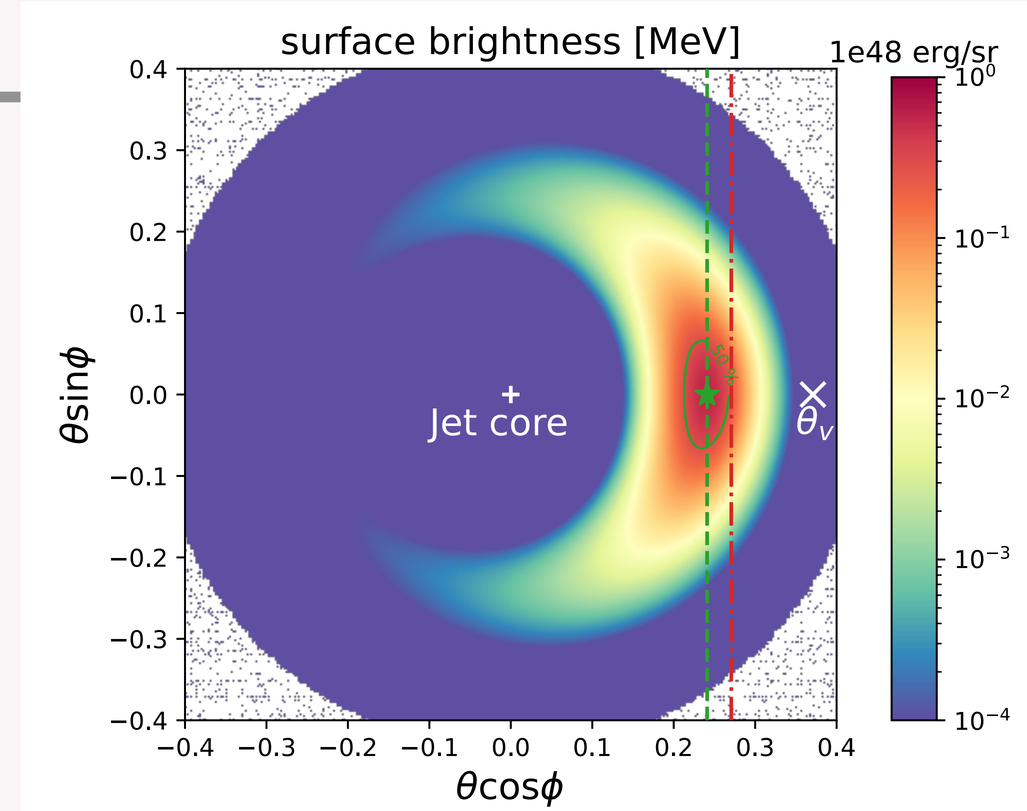

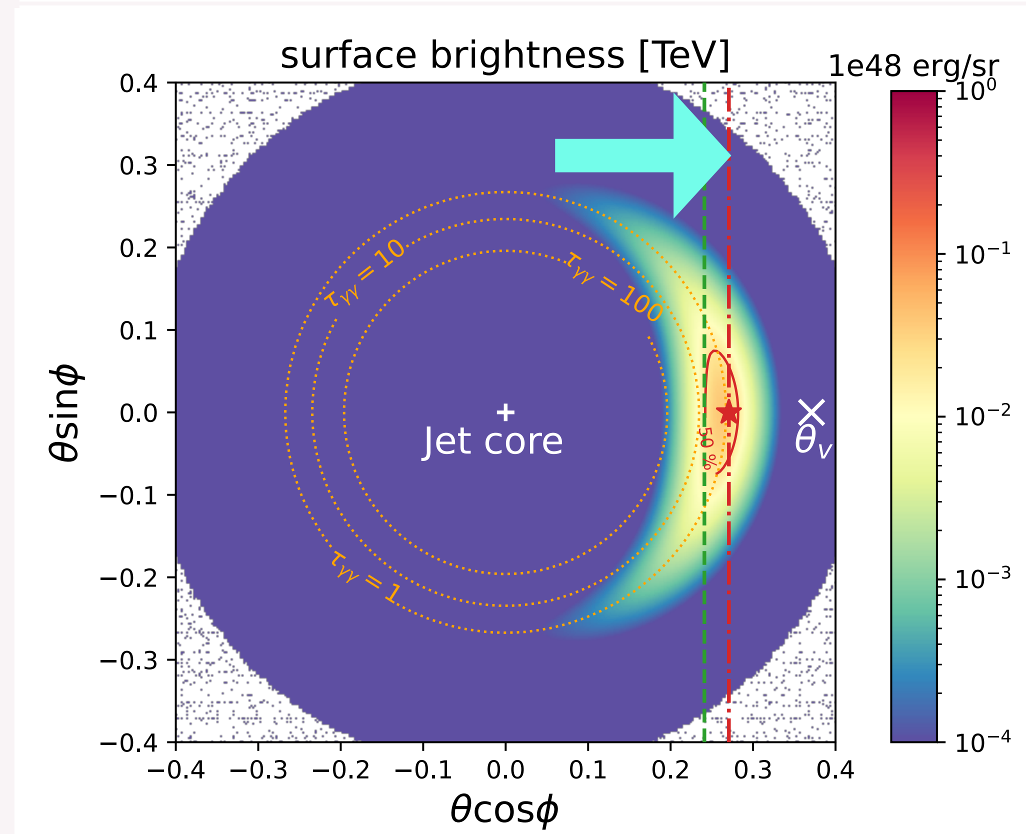

Emission regions with 50% surface brightness are shifted between the MeV and TeV bands!

Off-axis MeV and very-high energy gamma-ray emissions from structured gamma-ray burst jets

- **MeV/TeV photons**

The optical depth is sensitive to the emission radius: the corresponding time delay between the typical arrival time of the TeV and MeV emission decreases with the increase of the emission radius.

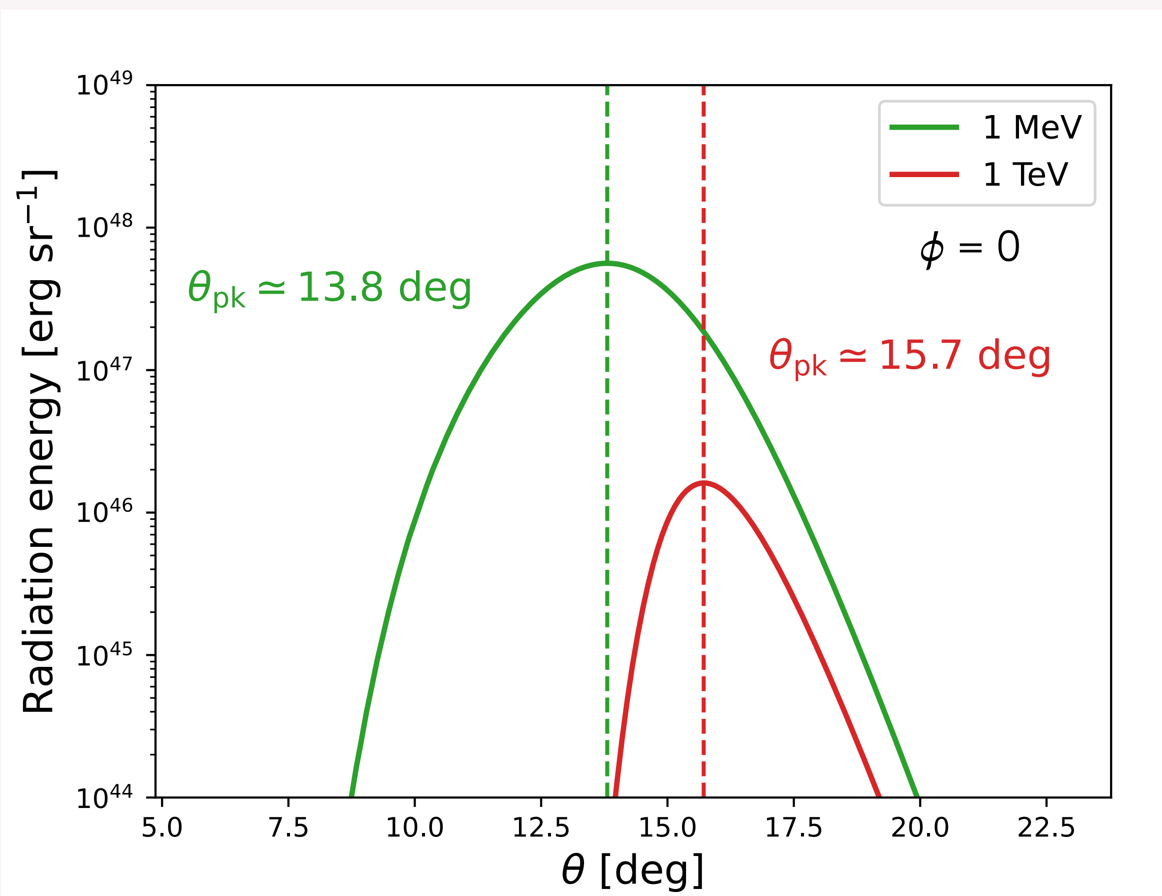

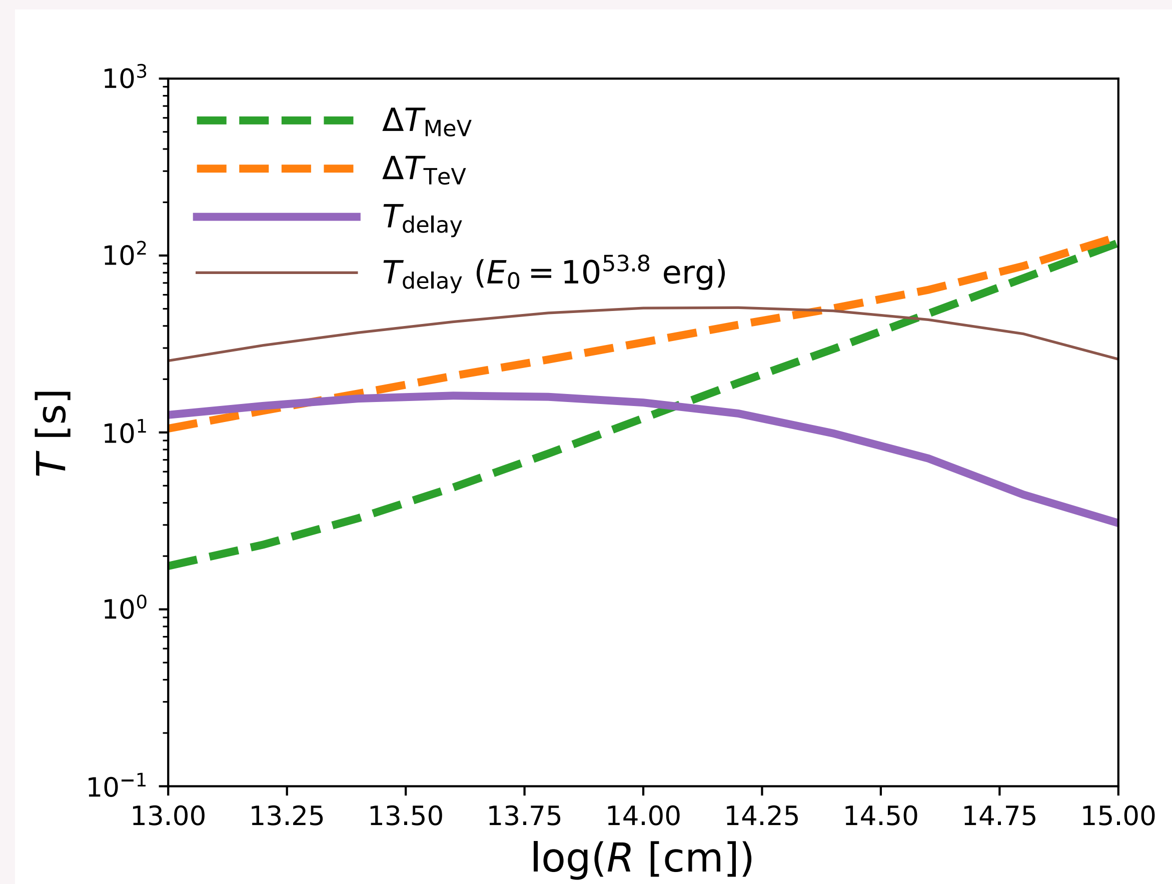

ŽB, Zhang, Murase, Ioka 2024

The typical arrival time of VHE photons could be delayed compared to the typical arrival time of prompt sub-MeV/MeV photons

Summary - I

→ We selected 3 representative reference events out of the sample of detected LL GRBs (GRB 980425, GRB 100316D, GRB 120714B), and modelled the three prototypes based on these reference events: a single-peaked GRB of medium peak energy (sp-GRB), ultra-long multipeaked GRB (ul-GRB) and a single-peaked GRB with higher luminosity and redshift (hl-GRB).

→ We found that LL GRBs are indeed potential targets for multimessenger observtaions and could be detected by current/future IACTs: this is mainly due to their **low redshifts (and high local rate) which reduce the effect of EBL absorption at the HE**

→ **The intensity of the HE component is linked to the magnetic field strength**

→ **LL GRBs are able to accelerate nuclei to the UHE: the maximal energies of iron nuclei (protons) could be as high as ≃ 10^{11} GeV (10^{10} GeV). The highes maximal energies were achieved for large magnetic fields, for which the IC efficiency is low**

Summary - II

→ We studied the radiative signatures of cosmic-ray protons in the prompt phase of energetic GRBs. We found that hadronic signatures appear as corelated flux increases in the optical-UV to soft X-ray and GeV to TeV gamma-ray ranges in the synchrotron scenarios

When the characteristic decay length of the magnetic field ($B \propto e^{-t'/t_B'}$) is significantly shorter than the dynamical scale (t_B'/t_{dyn}' ~ 0.01, 0.001) , the low energy prompt GRB synchrotron spectrum becomes significantly harder. The regime of marginally fast cooling is naturally achieved

When considering the off-axis structured jets, we found that **different energy photons could arrive from different emission zones,** mainly due to the effect of the two-photon pair annihilation process. The optical depth for VHE photons is sensitive to the emission radius, where the corresponding **time delay between the typical arrival time of the TeV and MeV emission** decreases with the increase of the emission radius.